ORNL/TM-2021/5

Preirradiation Characterization of MiniFuel Compacts for High-Power Irradiation Testing of TRISO Fuel

Tyler J. Gerczak
Grant W. Helmreich
Christopher A. Hobbs
Andrew K. Kercher
Ryan Latta

January 2021

Approved for public release.
Distribution is unlimited

OAK RIDGE NATIONAL LABORATORY
MANAGED BY UT-BATTELLE FOR THE US DEPARTMENT OF ENERGY

ORNL/TM-2021/5

Nuclear Energy and Fuel Cycle Division

Fabrication of MiniFuel Compacts for High-Power Irradiation Testing of TRISO Fuel

Tyler J. Gerczak
Grant W. Helmreich
Christopher A. Hobbs
Andrew K. Kercher
Ryan Latta

Date Published: January 2021

Prepared by
OAK RIDGE NATIONAL LABORATORY
Oak Ridge, TN 37831-6283
managed by
UT-BATTELLE, LLC
for the
US DEPARTMENT OF ENERGY
under contract DE-AC05-00OR22725

CONTENTS

LIST OF FIGURES

LIST OF TABLES

ACRONYMS

AGR	Advanced Gas Reactor
DOE	US Department of Energy
FHR	Fluoride Salt-Cooled High-Temperature Reactor
HFIR	High Flux Isotope Reactor
HTGR	high-temperature gas cooled reactor
KP	Kairos Power LLC
LEUCO	low-enriched UCO
$LEUO_2$	low-enriched UO_2
NUCO	natural uranium UCO
ORNL	Oak Ridge National Laboratory
PIE	postirradiation examination
TRISO	tristructural isotropic
UCO	uranium oxide, uranium carbide
UO_2	uranium oxide
XCT	x-ray computed tomography

ACKNOWLEDGMENTS

This research was sponsored by the Nuclear Science User Facilities Program of the US Department of Energy (DOE), Office of Nuclear Energy. The report was authored by UT-Battelle under Contract No. DE-AC05-00OR22725 with DOE.

ABSTRACT

MiniFuel compacts containing 20 individual tristructural isotropic (TRISO)-coated fuel particles were characterized to provide supporting preirradiation characterization data. The preirradiated characterization data supports irradiation capsule design and safety analysis, as well as downstream postirradiation examination (PIE) for a planned MiniFuel irradiation to explore high particle powers. The analysis included dimensional inspection, x-ray radiography and tomography, as-fabricated defect fraction analysis, and a matrix impurity analysis.

1. INTRODUCTION

The performance of tristructural isotropic (TRISO)-coated particle fuel has been established for operating conditions that are typical of high-temperature gas cooled reactors (HTGR) where modern TRISO fuel irradiation experiments have demonstrated failure fractions below design limits at typical HTGR conditions (Demkowicz et al. 2019). The successful demonstration of TRISO fuel for HTGR concepts has led to interest in the TRISO fuel concept for application outside HTGRs due to the robustness of the coated particle fuel architecture. TRISO fuel and TRISO fuel-related concepts are currently under consideration for accident-tolerant light water reactor concepts (Terrani et al. 2012) and molten salt reactor concepts (Brown et al. 2017). These novel designs could explore conditions not typically associated with HTGR operations, such as temperature, fluence, burnup, and power density.

The Kairos Power LLC (KP) Fluoride Salt-Cooled High-Temperature Reactor (FHR) design represents a novel reactor design that uses TRISO fuel particles. The reactor concept leverages a spherical pebble fuel form in a molten salt coolant. This approach effectively couples two Generation IV reactor technologies. The design varies from HTGR concepts in that the properties of the molten salt allow for higher power densities. Also, the potential for the salt coolant to accommodate fission products may support higher particle failure rates compared with traditional HTGRs. The opportunity to operate at higher power densities requires an understanding of particle performance at higher particle powers relative to what has traditionally been explored in HTGR supporting irradiations. An irradiation experiment was developed to explore particle powers at FHR-relevant temperatures for particle powers that bound the operational envelope for very high-power density FHR designs (Latta et al. 2020). The irradiation will be conducted in the High Flux Isotope Reactor (HFIR) at Oak Ridge National Laboratory (ORNL). This experiment is expected to demonstrate TRISO fuel performance at margin conditions to establish the bounding behavior for high particle power operation.

Two distinct comparisons are included in the planned experiment. The first is a comparison between TRISO particles at different particle powers at FHR-relevant operational conditions. Average particle powers are expected to range from ~70–600 mW and will be tested at two temperatures: 500 and 700°C. The range in average particle power is influenced by TRISO particle enrichment and will be confirmed through detailed neutronics calculations as part of the irradiation design process. Two different particle types are included: one with kernels with mixed low-enriched uranium oxide and uranium carbide (UCO) kernels and one with natural enriched UCO kernels. The low-enriched particles represent the higher particle power variant, whereas the natural-enriched UCO TRISO particles represent the low particle power range. These two variants are designated as *LEUCO* and *NUCO*, respectively. The conditions explored here bound the particle powers explored by the US Department of Energy (DOE) Advanced Gas Reactor Fuel Qualification and Development (AGR) program's second irradiation experiment AGR-2 (Collin 2014). The second comparison is concerned with potential kernel migration at the higher particle powers. Kernel migration has been observed to be a failure mechanism in uranium oxide (UO_2) kernel particles (Homan et al. 1977). The degree of kernel migration is related to the size of the thermal gradients across the particles (Maki et al., 2007) and kernel migration can be mitigated by adding a

carbide phase to buffer $CO_{(g)}$ production (Bullock and Kaae 1983, McMurray et al., 2017). The impact of kernel composition on kernel migration will be explored by comparing low-enriched UCO (LEUCO) and low-enriched UO_2 kernel ($LEUO_2$) TRISO particles at similar particle powers irradiated at nominally 900°C.

This report describes the particles and compacted fuel forms to be irradiated and the associated preirradiation characterization completed to support the irradiation design and approval. The irradiation capsule design is discussed in a separate report by Gallagher et al. (2020).

2. SAMPLE DESCRIPTION

Three variants were identified to be included in the planned irradiation experiment. The irradiation capsule design leveraged the novel MiniFuel irradiation approach to support the separate effects testing of small fuel volumes (Petrie et al. 2019). A small modification to the irradiation capsule design was incorporated into this experiment to explore small-volume "compacts" to avoid single-point heat conduction and atypical thermal gradients. The compact fabrication process was not optimized beyond providing a 3D heat conduction pathway and ensuring no particles were compromised during fabrication. Particles selected for irradiation were obtained from the existing inventory of particles from the AGR program. These particles were upgraded for roundness via tabling and subsequently compacted into MiniFuel compacts to meet the irradiation capsule design criteria. A total of 20 particles per compact were targeted based on initial neutronics and thermal analysis which was used to optimize the number of particles included in the irradiation to increase particle statistics while limiting particle-to-particle variation in irradiation temperature and particle power. The development and fabrication of the MiniFuel compacts were supported by KP through a Strategic Partnership Program (Gerczak et al. 2020).

2.1 TRISO PARTICLES

Particles selected for irradiation were associated with the second AGR irradiation experiment, AGR-2. Because of this pedigree, significant preirradiation characterization has been completed on the kernel and particle properties. Table 1 and Table 2 list the relevant kernel and particle properties for the particles included in this irradiation experiment. Collin (2014) compiled the data, and the source data were provided by BWXT documents (2008a, 2008b, 2008c, 2009) and two documents by Hunn et al. (2008, 2010). The particle lots for the LEUCO (LEU09) and $LEUO_2$ (LEU11) particles were the same as those included in the AGR-2 irradiation experiment, whereas the NUCO (NUCO425-08T) particles were produced before the start of the LEUCO particles coating efforts to establish optimal coating conditions. The NUCO kernels and particles did not receive the same focus as the LEU09 and LEU11 sample sublots because they were not intended to be included in the AGR irradiation campaign. Select values for the NUCO kernels and particles are reported in Table 1 and Table 2, and select values and kernel enrichment were reported previously by Seibert et al. (2019). The mean values reported for NUCO425-08T particle properties in Table 1 and Table 2 were measured to the same standards as the LEU09 and LEU11 particles following AGR program procedures; however, a formal ORNL data package report has not yet been published. Additional NUCO kernel analysis was completed in this effort which focused on kernel phase fraction.

Table 1. Reported relevant kernel properties of particles used in the fabrication of MiniFuel compacts.

Variant	LEUCO	$LEUO_2$	NUCO
Sublot designation	G73I-14-69307	G73AA-10-69308	-
Diameter (μm)	426.7 ± 8.8	507.7 ± 11.9	422.4 ± 13.8
Density (Mg/m^3)	10.966 ± 0.033	10.858 ± 0.082	10.58 ± 0.35*
^{235}U enrichment (wt %)	14.029 ± 0.026	9.600 ± 0.010	0.71
Carbon/uranium (atomic ratio)	0.392 ± 0.002	N/A	0.432 ± 0.031*
Oxygen/uranium (atomic ratio)	1.428 ± 0.005	2.003 ± 0.005	1.512 ± 0.036*
[Carbon + oxygen]/uranium (atomic ratio)	1.818 ± 0.005	N/A	1.944 ± 0.004*
Total uranium (wt %)	89.463 ± 0.051	N/A	89.010 ± 0.001*
Sulfur impurity (ppm – wt)	365 ± 12	≤50	N/A
Phosphorus impurity (ppm – wt)	≤50		N/A
All other impurities	Below minimum detection limits and within specification		N/A

* values measured by automated image analysis
± values reported as one standard deviation from the mean

Table 2. Reported relevant particle properties of particles used in the fabrication of MiniFuel compacts.

Variant	LEUCO	$LEUO_2$	NUCO
Lot designation	LEU09	LEU11	NUCO425-08T
Buffer thickness (μm)	98.9 ± 8.4	97.7 ± 9.9	106.1 ± 10.9
IPyC thickness (μm)	40.4 ± 2.5	41.9 ± 3.2	44.4 ± 2.8
SiC thickness (μm)	35.2 ± 1.2	37.5 ± 1.2	34.9 ± 1.1
OPyC thickness (μm)	43.4 ± 2.9	45.6 ± 2.4	40.3 ± 2.9
Buffer density (Mg/m^3)	Not measured	0.99	Not measured
IPyC density (Mg/m^3)	1.890 ± 0.011	Not measured	Not measured
SiC density (Mg/m^3)	3.197 ± 0.004	3.199	3.188 ± 0.002
OPyC density (Mg/m^3)	1.907 ± 0.007	1.884 ± 0.004	1.903 ± 0.004
IPyC anisotropy (BAF)	1.0349 ± 0.0012	1.0334 ± 0.0027	1.0400 ± 0.0015
OPyC anisotropy (BAF)	1.0263 ± 0.0011	1.0219 ± 0.0012	1.0276 ± 0.0010
SiC sphericity (aspect ratio)	1.037 ± 0.011	1.034 ± 0.010	Not measured
OPyC sphericity (aspect ratio)	1.052	1.052	1.058
Particle diameter (μm)	873.2 ± 23	953.0 ± 28	870.40 ± 22
Mean particle mass (mg)	1.032 ± 0.003	1.462 ± 0.005	1.016 ± 0.002

± values reported as one standard deviation from the mean

The phase fraction data for the carbon/uranium, oxygen/uranium, [carbon + oxygen]/uranium, and total uranium for the NUCO kernels were measured on full TRISO particles, not kernel sublots, as part of the preirradiation characterization effort for MiniFuel compact analysis. Phase fraction and density data were

measured on a per-kernel basis for approximately 100 NUCO425-08T kernels from full TRISO particles by using previously developed automated image analysis software (Helmreich et al. 2020a). This method segments cross-sectional images of UCO kernels, polished to a known depth, into carbide, oxide, and void phases based on scanning electron microscopy backscatter electron image intensity. These segmented images are analyzed with their known polish-down distances to accurately determine the volumetric fractions for each phase. These volumetric phase fractions can then be converted to atomic or weight fractions and used to calculate overall kernel density if the stoichiometry of the carbide phase is known. Figure 1 shows an example of the analysis process for a single particle where yellow is the oxide phase, teal is the carbide phase, and dark blue is the void space. The carbide phase was assumed to be 90% uranium dicarbide and 10% uranium monocarbide. The acquired data are reported in Table 1. Differences in the atomic ratios and kernel density were observed when comparing the data from the LEUCO and NUCO kernels. The reported differences are expected to be associated with the variation in analysis approaches and the fact that one set of analysis was conducted on as-fabricated kernels and the other on coated kernels. Specifically, the lower density was speculated to be resultant from excess void space due to pullout from mechanical sample preparation particularly near the kernel rind. Other artifacts may be resultant from the assumed uranium monocarbide fraction.

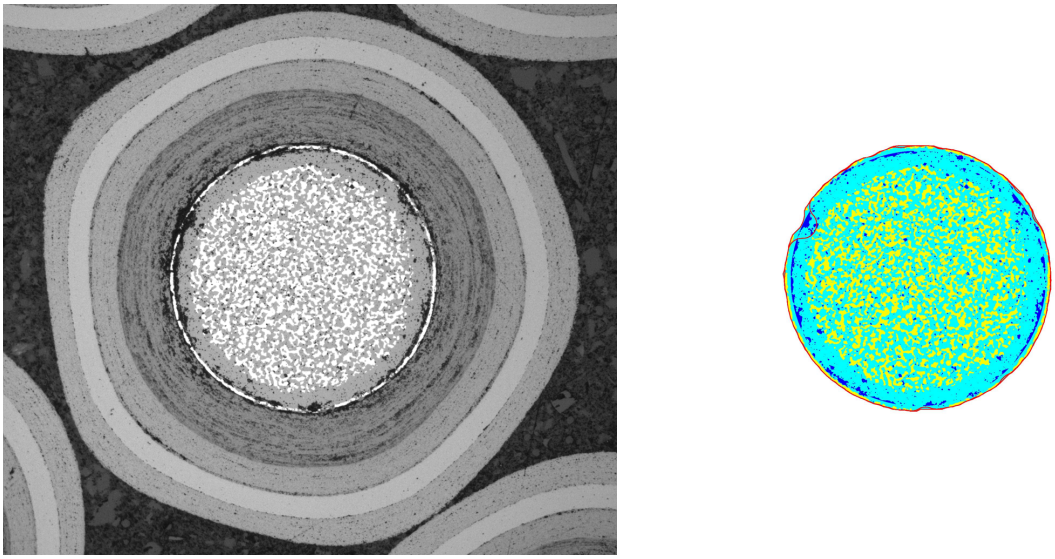

Figure 1. Example of optical image used for kernel compositional analysis (left) and segmented phases from image analysis (right).

2.2 COMPACT DESCRIPTION

MiniFuel compacts were produced to provide a 3D heat transfer medium to avoid single-point contact with a sample holder and unintended directional thermal gradients across the particles. KP sponsored the compact fabrication under the strategic partnership project NFE-19-07790 to provide support for “Mini-Compact Development for High Power Irradiation testing of TRISO Fuel” in accordance with defined statement of work. The MiniFuel compacts represent the final fuel form that will be inserted into the irradiation capsule build. The preirradiation characterization of the MiniFuel compacts was completed to support the capsule build and approval process, refine thermal models, and support downstream postirradiation examination (PIE) efforts.

2.2.1 Compact Fabrication Summary

The MiniFuel compact fabrication process was reported in the sponsor-controlled report ORNL/SPR-2020/1778 (Gerczak et al. 2020), and this section provides a generic overview. The compacting process leveraged techniques and equipment similar to those used to produce compacts for the AGR program (Pappano et al. 2008). The general process consisted of upgrading particles, overcoating particle sublots, pressing green compacts, carbonizing compacts, and performing a final high-temperature heat treatment. Small sublots of particles were riffled out from larger particle volumes to obtain a randomly representative distribution of particles, then upgraded by hand-tabling to remove faceted or other nonideal particles.

Particles were overcoated to predetermined overcoated particle weight targets to form a 20 particle charge for pressing a green compact. Particles were overcoated by using materials and processes that were consistent with compact fabrication from AGR-1 to AGR-4 (Hunn et al. 2010a, Hunn et al. 2010b, Hunn et al. 2014, Pappano et al. 2008, Pappano and Hunn 2008). The matrix was prepared at ORNL. The matrix composition used was similar to the A3-3 refence materials and comprised natural graphite flake, synthetic graphite flake, and a resin binder in a 64:16:20 mass ratio (Gerczak et al. 2020).

A lab-scale overcoater was used to over coat the particles of interest. The system comprised an overcoating drum, ultrasonic atomizer, and syringe pump. A green compact matrix density of ~1.45 g/cm^3 was targeted to meet the final matrix density targets of 1.22–1.34 g/cm^3. This range in final density represents the range in densities found in the AGR-1 irradiation experiment (Hunn et al. 2012). The higher green density accounts for the resin binder volatilization during carbonization and high-temperature heat treatment which leads to a reduction in density after the carbonization step. The green compact weight was used to target average overcoated particle weight and the ultimate 20 particle charge weight.

Overcoated particles were separated into separate bins based on particle diameter by using a roller micrometer. The average particle weight per bin was measured and used to produce 20 particle charges for pressing MiniFuel compacts. Pressing was conducted by using a Promess Inc. automated servo-driven mechanical press and a custom single-acting die and punch set. Pressing was done at a die temperature of 60°C, and the press height was controlled to fabricate reproducible compact thicknesses. A peak pressing force limit was set at 200 lb, which reflects ~7,800 psi. This force exceeds the compact pressing pressure of ~2,700 psi explored in the AGR program and the maximum peak forces measured during pressing of MiniFuel compacts were ~2,445 psi.

Green compacts were then subjected to carbonization and a heat-treatment schedule similar to those used to fabricate AGR-1 through AGR-4 compacts (AGR-COMP-SOP-05 Rev. 1 and AGR-CHAR-SOG-27). The carbonization step involved thermal exposure at ~950°C for 1 h under flowing inert gas. This process partially carbonizes the resin binder and drives out volatile components. After carbonization, the MiniFuel compacts were subjected to a high-temperature heat treatment at 1,800°C for ~1 h. This step drives out impurity elements and further carbonizes the resin. Afterward, fabrication compacts were subjected to a series of characterizations to provide data relevant to the irradiation planning and downstream PIE.

3. FINAL COMPACT PROPERTIES

3.1 COMPACT DIMENSION ANALYSIS

An analysis was performed on all produced compacts to measure the weight and dimension and to calculate density. The methods for measuring these properties were based on established procedures from the AGR program (AGR-CHAR-DAM-42, Rev. 1) that were modified slightly due to the unique geometry of these samples. The compact dimensions were measured using a Mitotuyo digital caliper to measure the diameter and a Starrett digital height gauge to measure the compact thickness. The compact weight was measured by using a Mettler Toledo digital balance. The matrix density was calculated by isolating the matrix volume, and the weight was determined by subtracting the volume and weight of 20 particles by using the average particle properties in Table 2. The calculated matrix density was a primary down-selection criterion for identifying compacts for irradiation and archiving samples. Specifically, outlier densities were excluded to control for this property. Other down-selection criteria are discussed in Section 3.2.1. Compacts that were not selected for irradiation or archive were subjected to burn testing for as-fabricated particle defect analysis (Section 3.2.3). Most compacts from the LEUCO-M##G series were subjected to burn testing because these were produced specifically to supply compacts for defect analysis. Select compacts, designated as "Yes" in the XCT column of Table 3–Table 6, were subjected to 3D x-ray computed tomography (XCT) analysis to support downstream PIE and the refinement of thermal models (Section 3.2.2).

Table 3. Post-heat-treatment compact properties for NUCO variant compacts (Series M##F).

Compact ID	Weight (g)	Height (mm)	Dia. (mm)	ρ (g/cm^3)	Matrix ρ (g/cm^3)	Status	XCT
NUCO-M01F	0.0627	2.33	4.55	1.6550	1.3690	Archive/Irradiation	Yes
NUCO-M02F	0.0598	2.31	4.54	1.5991	1.2959	Archive/Irradiation	Yes
NUCO-M03F	0.0591	2.30	4.55	1.5803	1.2729	Archive/Irradiation	No
NUCO-M04F	0.0601	2.31	4.55	1.6001	1.2987	Archive/Irradiation	Yes
NUCO-M05F	0.0594	2.32	4.55	1.5747	1.2692	Archive/Irradiation	Yes
NUCO-M06F	0.0592	2.31	4.56	1.5692	1.2626	Archive/Irradiation	Yes
NUCO-M07F	0.0597	2.30	4.54	1.6034	1.2995	Archive/Irradiation	Yes
NUCO-M08F	0.0607	2.30	4.54	1.6303	1.3325	Archive/Irradiation	No
Min	0.0591	2.30	4.54	1.5692	1.2626	-	-
Max	0.0627	2.33	4.56	1.6550	1.3690	-	-
Mean	0.0601	2.31	4.55	1.6015	1.3001	-	-
Standard dev.	0.0012	0.01	0.01	0.0291	0.0357	-	-

Table 4. Post-heat-treatment compact properties for LEUCO variant compacts (Series M##E).

Compact ID	Weight (g)	Height (mm)	Dia. (mm)	ρ (g/cm^3)	Matrix ρ (g/cm^3)	Status	XCT
LEU09-M01E	0.0626	2.37	4.59	1.5963	1.3013	Archive/Irradiation	Yes
LEU09-M02E	0.0614	2.36	4.58	1.5792	1.2774	Archive/Irradiation	No
LEU09-M03E	0.0618	2.37	4.58	1.5828	1.2833	Archive/Irradiation	No
LEU09-M04E	0.0631	2.36	4.60	1.6088	1.3166	Burn test	No
LEU09-M05E	0.0620	2.36	4.58	1.5946	1.2962	Burn test	No
LEU09-M06E	0.0611	2.35	4.58	1.5782	1.2746	Archive/Irradiation	No
LEU09-M07E	0.0615	2.34	4.57	1.6023	1.3008	Archive/Irradiation	Yes
LEU09-M08E	0.0621	2.35	4.57	1.6110	1.3131	Archive/Irradiation	No
LEU09-M09E	0.0604	2.34	4.56	1.5805	1.2726	Archive/Irradiation	No
LEU09-M10E	0.0628	2.36	4.58	1.6152	1.3213	Archive/Irradiation	No
LEU09-M11E	0.0633	2.37	4.58	1.6212	1.3301	Archive/Irradiation	No
LEU09-M12E	0.0617	2.34	4.59	1.5935	1.2933	Burn test	No
LEU09-M13E	0.0624	2.33	4.59	1.6185	1.3223	Archive/Irradiation	No
LEU09-M14E	0.0622	2.36	4.58	1.5998	1.3025	Archive/Irradiation	Yes
LEU09-M15E	0.0611	2.34	4.58	1.5849	1.2812	Burn test	No
LEU09-M16E	0.0620	2.34	4.57	1.6153	1.3167	Archive/Irradiation	No
LEU09-M17E	0.0615	2.34	4.59	1.5883	1.2870	Archive/Irradiation	No
LEU09-M18E	0.0625	2.35	4.57	1.6214	1.3257	Archive/Irradiation	No
LEU09-M19E	0.0620	2.35	4.57	1.6084	1.3099	Archive/Irradiation	Yes
LEU09-M20E	0.0624	2.34	4.58	1.6186	1.3224	Archive/Irradiation	No
LEU09-M21E	0.0629	2.35	4.58	1.6247	1.3313	Archive/Irradiation	No
LEU09-M22E	0.0609	2.34	4.58	1.5797	1.2749	Archive/Irradiation	No
LEU09-M23E	0.0606	2.33	4.57	1.5856	1.2789	Burn test	No
LEU09-M24E	0.0618	2.34	4.58	1.6031	1.3034	Archive/Irradiation	Yes
LEU09-M25E	0.0614	2.32	4.58	1.6064	1.3043	Archive/Irradiation	No
LEU09-M26E	0.0616	2.33	4.57	1.6118	1.3109	Archive/Irradiation	Yes
LEU09-M27E	0.0605	2.34	4.57	1.5762	1.2690	Archive/Irradiation	No
LEU09-M28E	0.0636	2.35	4.59	1.6356	1.3462	Burn test	No
LEU09-M29E	0.0626	2.36	4.58	1.6101	1.3150	Archive/Irradiation	Yes
LEU09-M30E	0.0635	2.36	4.60	1.6190	1.3290	Burn test	No
LEU09-M31E	0.0605	2.32	4.57	1.5898	1.2824	Burn test	No
LEU09-M32E	0.0613	2.33	4.58	1.5969	1.2943	Archive/Irradiation	No
LEU09-M33E	0.0612	2.33	4.57	1.6013	1.2981	Burn test	No
LEU09-M34E	0.0628	2.33	4.59	1.6289	1.3349	Archive/Irradiation	No
LEU09-M35E	0.0610	2.32	4.57	1.6029	1.2985	Archive/Irradiation	No
LEU09-M36E	0.0623	2.35	4.59	1.6022	1.3054	Archive/Irradiation	Yes
LEU09-M37E	0.0624	2.35	4.59	1.6047	1.3086	Burn test	No
LEU09-M38E	0.0612	2.35	4.58	1.5807	1.2777	Archive/Irradiation	No
LEU09-M39E	0.0612	2.34	4.58	1.5875	1.2844	Archive/Irradiation	No
LEU09-M40E	0.0611	2.34	4.59	1.5780	1.2744	Burn test	No
LEU09-M41E	0.0607	2.34	4.58	1.5745	1.2686	Archive/Irradiation	No
LEU09-M42E	0.0623	2.34	4.58	1.6160	1.3192	Archive/Irradiation	Yes
LEU09-M43E	0.0606	2.37	4.58	1.5520	1.2459	Burn test	No
LEU09-M44E	0.0609	2.37	4.58	1.5597	1.2553	Burn test	No
LEU09-M45E	0.0603	2.36	4.56	1.5645	1.2563	Archive/Irradiation	No
LEU09-M46E	0.0605	2.34	4.58	1.5693	1.2622	Archive/Irradiation	No
LEU09-M47E	0.0600	2.34	4.58	1.5564	1.2464	Burn test	No
Min	0.0600	2.32	4.56	1.5520	1.2459	-	-
Max	0.0636	2.37	4.60	1.6356	1.3462	-	-
Mean	0.0617	2.35	4.580	1.5965	1.2963	-	-
Standard dev.	0.0009	0.014	0.009	0.0200	0.0246	-	-

Table 5. Post-heat-treatment compact properties for LEUCO variant compacts (Series M##G).

Compact ID	Weight (g)	Height (mm)	Dia. (mm)	ρ (g/cm^3)	Matrix ρ (g/cm^3)	Status	XCT
LEU09-M02G	0.0615	2.360	4.58	1.5818	1.2805	Burn test	No
LEU09-M03G	0.0640	2.361	4.60	1.6332	1.3460	Archive/Irradiation	No
LEU09-M04G	0.0612	2.361	4.60	1.5620	1.2593	Burn test	No
LEU09-M05G	0.0635	2.371	4.59	1.6160	1.3260	Burn test	No
LEU09-M06G	0.0632	2.354	4.59	1.6225	1.3309	Burn test	No
LEU09-M07G	0.0631	2.358	4.59	1.6146	1.3224	Burn test	No
LEU09-M08G	0.0625	2.358	4.58	1.6065	1.3109	Burn test	No
LEU09-M09G	0.0617	2.368	4.58	1.5813	1.2813	Burn test	No
LEU09-M10G	0.0641	2.359	4.60	1.6376	1.3510	Archive/Irradiation	No
LEU09-M11G	0.0635	2.363	4.60	1.6146	1.3247	Burn test	No
LEU09-M12G	0.0632	2.373	4.60	1.6026	1.3110	Burn test	No
LEU09-M13G	0.0641	2.375	4.59	1.6332	1.3466	Burn test	No
LEU09-M14G	0.0627	2.371	4.59	1.6005	1.3061	Burn test	No
LEU09-M15G	0.0638	2.359	4.59	1.6345	1.3461	Burn test	No
LEU09-M16G	0.0640	2.354	4.60	1.6359	1.3487	Burn test	No
LEU09-M17G	0.0636	2.359	4.57	1.6412	1.3518	Burn test	No
LEU09-M18G	0.0631	2.356	4.58	1.6278	1.3356	Burn test	No
LEU09-M19G	0.0642	2.359	4.60	1.6397	1.3536	Burn test	No
LEU09-M20G	0.0623	2.358	4.59	1.5990	1.3023	Burn test	No
LEU09-M21G	0.0641	2.354	4.59	1.6433	1.3566	Burn test	No
LEU09-M22G	0.0628	2.356	4.58	1.6156	1.3217	Burn test	No
LEU09-M23G	0.0629	2.361	4.60	1.6056	1.3123	Burn test	No
LEU09-M24G	0.0644	2.363	4.59	1.6473	1.3623	Archive/Irradiation	No
LEU09-M25G	0.0625	2.358	4.57	1.6138	1.3181	Burn test	No
LEU09-M26G	0.0624	2.359	4.58	1.6035	1.3073	Burn test	No
LEU09-M27G	0.0632	2.377	4.59	1.6045	1.3129	Burn test	No
LEU09-M28G	0.0628	2.354	4.59	1.6148	1.3209	Burn test	No
LEU09-M29G	0.0645	2.380	4.59	1.6404	1.3559	Burn test	No
LEU09-M30G	0.0625	2.334	4.59	1.6183	1.3227	Burn test	No
LEU09-M31G	0.0627	2.378	4.57	1.6051	1.3106	Burn test	No
LEU09-M32G	0.0641	2.375	4.60	1.6264	1.3397	Burn test	No
LEU09-M33G	0.0630	2.363	4.58	1.6183	1.3255	Burn test	No
LEU09-M34G	0.0641	2.366	4.59	1.6352	1.3485	Burn test	No
LEU09-M35G	0.0637	2.360	4.59	1.6334	1.3445	Burn test	No
LEU09-M36G	0.0630	2.348	4.59	1.6218	1.3290	Burn test	No
LEU09-M37G	0.0633	2.364	4.58	1.6229	1.3318	Burn test	No
LEU09-M38G	0.0612	2.359	4.58	1.5727	1.2698	Burn test	No
LEU09-M39G	0.0621	2.357	4.59	1.5920	1.2942	Burn test	No
LEU09-M40G	0.0643	2.384	4.59	1.6324	1.3468	Burn test	No
LEU09-M41G	0.0621	2.369	4.56	1.6028	1.3049	Burn test	No
LEU09-M42G	0.0620	2.377	4.57	1.5876	1.2893	Burn test	No
LEU09-M43G	0.0611	2.366	4.59	1.5632	1.2598	Burn test	No
LEU09-M44G	0.0623	2.350	4.57	1.6160	1.3192	Burn test	No
LEU09-M45G	0.0613	2.342	4.58	1.5913	1.2887	Burn test	No
LEU09-M46G	0.0627	2.354	4.59	1.6074	1.3129	Burn test	No
Min	0.0611	2.334	4.56	1.5620	1.2593	-	-
Max	0.0645	2.384	4.60	1.6473	1.3623	-	-
Mean	0.0630	2.3619	4.587	1.6138	1.3209	-	-
Standard dev.	0.0009	0.010	0.01	0.0213	0.0263	-	-

Table 6. Post-heat-treatment compact properties for $LEUO_2$ variant compacts (Series M##B).

Compact ID	Weight (g)	Height (mm)	Dia. (mm)	ρ (g/cm^3)	Matrix ρ (g/cm^3)	Status	XCT
LEU11-M01B	0.0674	2.32	4.58	1.7634	1.3087	Archive/Irradiation	Yes
LEU11-M02B	0.0693	2.33	4.58	1.8053	1.3662	Burn test	No
LEU11-M03B	0.0693	2.33	4.59	1.7975	1.3584	Burn test	No
LEU11-M04B	0.0654	2.32	4.58	1.7111	1.2401	Burn test	No
LEU11-M05B	0.0671	2.31	4.58	1.7632	1.3058	Archive/Irradiation	Yes
LEU11-M06B	0.0689	2.33	4.58	1.7949	1.3525	Burn test	No
LEU11-M07B	0.0670	2.32	4.58	1.7529	1.2950	Burn test	No
LEU11-M08B	0.0670	2.33	4.58	1.7454	1.2877	Archive/Irradiation	No
LEU11-M09B	0.0670	2.33	4.58	1.7454	1.2877	Archive/Irradiation	No
LEU11-M10B	0.0662	2.33	4.58	1.7246	1.2604	Archive/Irradiation	No
LEU11-M11B	0.0661	2.32	4.58	1.7294	1.2641	Burn test	No
LEU11-M12B	0.0674	2.33	4.58	1.7558	1.3014	Archive/Irradiation	No
LEU11-M13B	0.0683	2.33	4.59	1.7715	1.3245	Archive/Irradiation	No
LEU11-M14B	0.0668	2.33	4.58	1.7402	1.2809	Archive/Irradiation	Yes
LEU11-M15B	0.0668	2.31	4.58	1.7553	1.2955	Archive/Irradiation	No
LEU11-M16B	0.0659	2.34	4.57	1.7169	1.2504	Burn test	No
LEU11-M17B	0.0651	2.32	4.58	1.7032	1.2298	Burn test	No
LEU11-M18B	0.0659	2.32	4.58	1.7242	1.2573	Burn test	No
LEU11-M19B	0.0654	2.32	4.59	1.7036	1.2331	Burn test	No
LEU11-M20B	0.0662	2.32	4.59	1.7245	1.2603	Archive/Irradiation	No
LEU11-M21B	0.0647	2.31	4.58	1.7001	1.2230	Burn test	No
LEU11-M22B	0.0648	2.34	4.56	1.6957	1.2198	Burn test	No
Min	0.0647	2.31	4.56	1.6957	1.2198	-	-
Max	0.0693	2.34	4.59	1.8053	1.3662	-	-
Mean	0.0667	2.325	4.580	1.7420	1.2819	-	-
Standard dev.	0.0013	0.009	0.007	0.0322	0.0430	-	-

3.2 X-RAY ANALYSIS

3.2.1 Particle Inventory Confirmation

All compacts considered for inclusion in the planned irradiation were screened to confirm the total number of particles and identify any potential defects or irregularities. Screening was completed by x-ray radiography via a Zeiss Versa 520 XCT instrument. Radiographs were taken along the axial direction of the right cylindrical compacts and at a 45° tilt from the axial direction. These two angles provided multiple perspectives to accurately count how many particles were in each compact. Example radiograph sets are show in Figure 2, Figure 3, and Figure 4 for NUCO, LEUCO, and $LEUO_2$ compacts, respectively. The LEU09-M##G series of compacts was not subjected to radiography analysis because they were provided exclusively for defect fraction analysis (Section 3.2.3). All radiography pairs used for particle count analysis are presented in Appendix A.

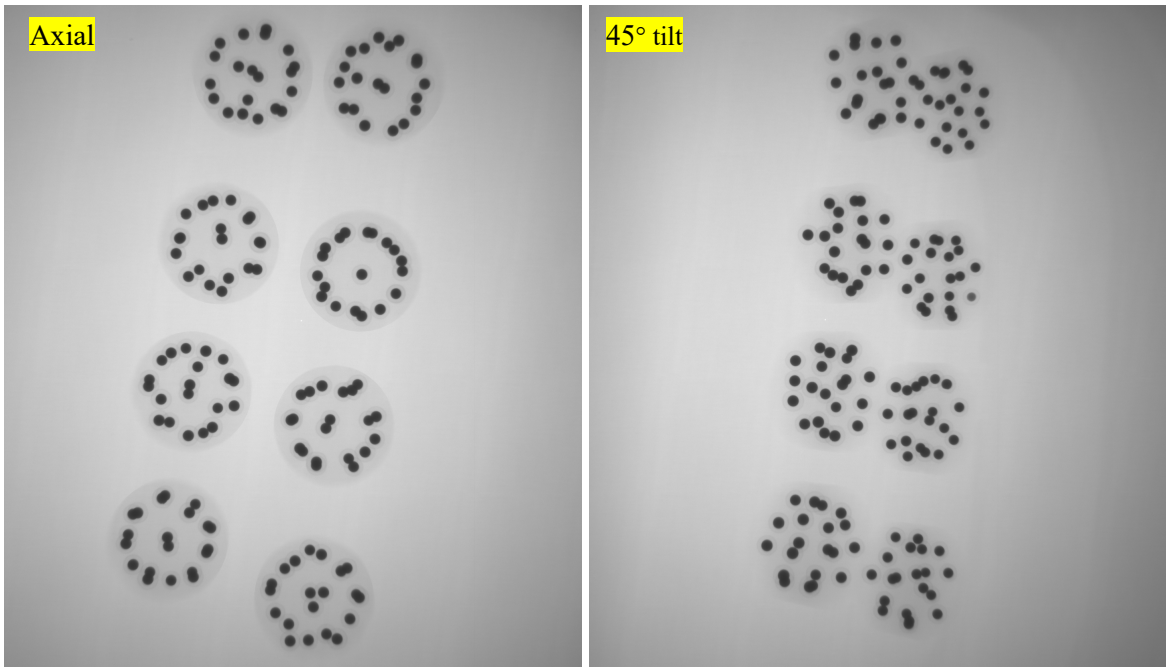

Figure 2. Example radiography sets of NUCO-M01F–NUCO-M08F.

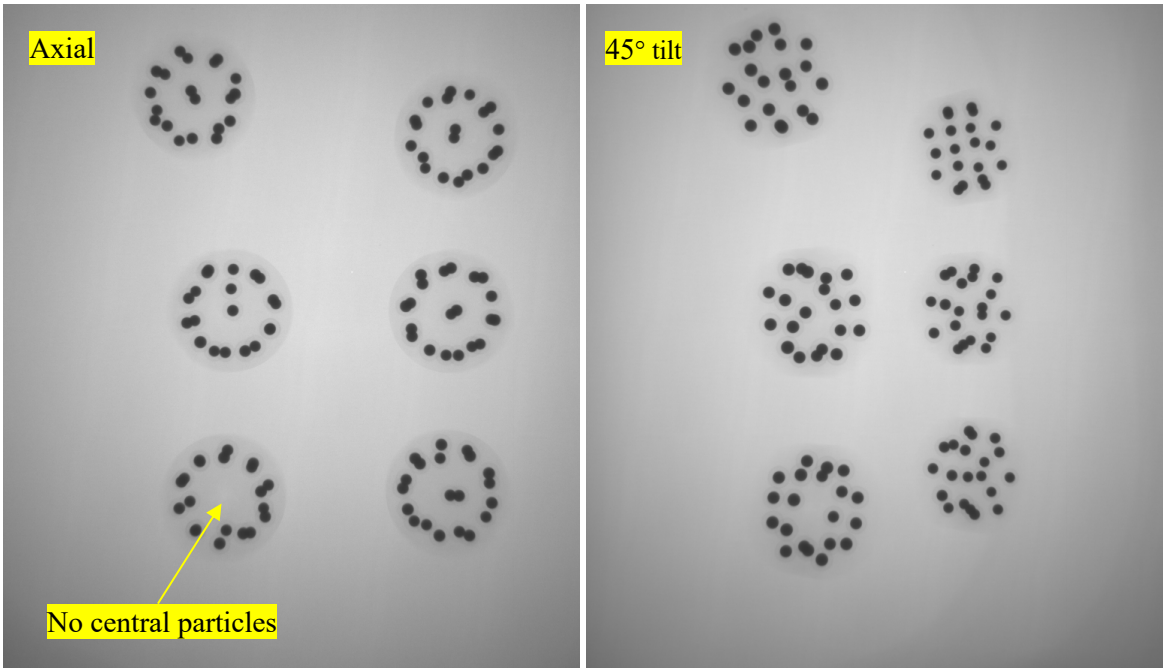

Figure 3. Example radiography sets of LEU09-M08E–LEU09-M12E.

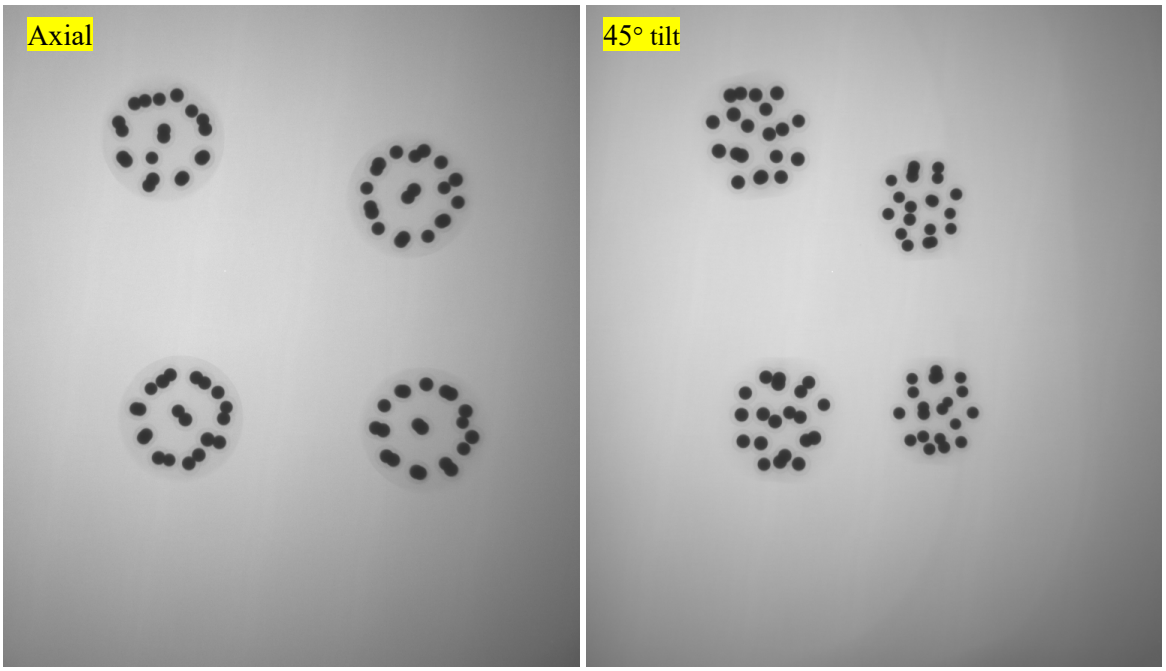

Figure 4. Example radiograph sets of LEU11-M05E–LEU11-M08E.

The radiography analysis provided two criteria to support compact down-selection in addition to density measurements discussed previously. If 20 particles were not clearly resolved in either of the two perspectives, then the compact was not considered for irradiation. This was the most common rejection criteria because particles were often observed to be overlapping. This rejection criterion was considered conservative. The second criterion was related to particle distribution. In select compacts in the LEU09-M##E series, a gap was observed in the center of the compacts as shown in Figure 3. This gap might not be critical; however, it represented an observed variation in particle distribution, and it was used to refine the compact variability in the planned test to ensure a more uniform set of compacts for irradiation.

The radiography confirmed 20 particles were present in all compacts selected for irradiation. Table 7 lists the total uranium content per MiniFuel compact based on average particle uranium content and enrichment.

Table 7. Total uranium content of MiniFuel compacts and isotopic breakdown.

		Weight per MiniFuel compact			
	Assay	**Total U (g)**	**^{234}U (g)**	**^{235}U (g)**	**^{238}U (g)**
LEUCO	0.710%	7.61E-03	3.93E-07	5.41E-05	7.57E-03
$LEUO_2$	14.174%	7.62E-03	7.16E-06	1.08E-03	6.53E-03
NUCO	9.580%	1.22E-02	7.47E-06	1.16E-03	1.10E-02

3.2.2 Particle Position Analysis

Select compacts were subjected to 3D XCT analysis (Table 3–Table 6). The whole compact tomography was conducted to support downstream PIE, particularly through refinement of thermal models to more accurately assess the compact and particle temperatures. The inputs that can be provided from 3D tomography analysis, specifically the particle positions and kernel volumes, will be used for thermal analysis to better predict the temperature distributions experienced across individual compacts as the current inputs assume a regular distribution of particles within the compact volume.

Each targeted compact was imaged by using a Zeiss Versa 520 XCT instrument. A series of 1,600 radiographs was acquired for each compact distributed over 360° of rotation with the x-ray source set to a maximum energy of 40 kV with no filter to maximize contrast of the low-Z graphite of the compact matrix. As shown in Figure 5, these settings sufficed to identify the outer edges of the compact and the positions of each kernel. Silicon carbide layers around each particle were partially distinguishable with some issues arising from image artifacts caused by the near-total blocking of x-rays by the high-Z kernels. These issues could be resolved by applying advanced model-based image reconstruction methods with beam-blocking corrections.

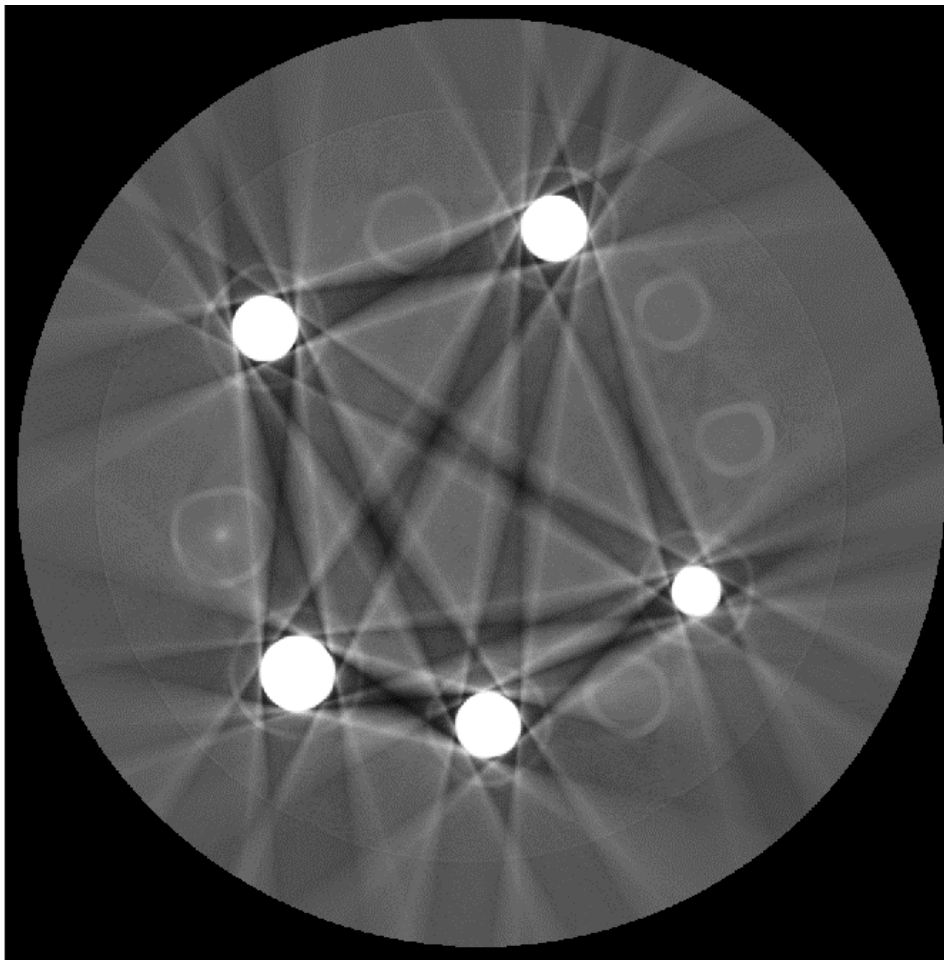

Figure 5. Cross-sectional tomogram from 3D tomograph of a compact showing kernels and SiC layers from several particles.

A previously developed software for analyzing XCT images of particle fuel forms was used to analyze each compact (Helmreich et al. 2020b). This software determined the centroid positions of each kernel relative to the body of the compact, as well as the volume of each kernel. Centroid data were then used to determine secondary parameters for each kernel. A watershed segmentation of the compact around each kernel centroid was used to determine the compact volume occupied by each particle, which can be used as a measure of extremely localized packing fraction. The distance from the centroid of each particle to the compact surface (surface distance) was calculated based on the automatic segmentation of the compact boundaries. Finally, the identity and distance (centroid to centroid) to the three nearest neighbors for each particle were determined. An example of the data generated for a single compact is given in Table 8. All XCT generated data from analyzed compacts is presented in Appendix B.

Table 8. XCT data for particles in compact NUCO-M01F.

Centroid (µm)			Volume (mm^3)		Surface distance (µm)	Nearest neighbor (µm)		
x	***y***	***z***	**Kernel**	**Region**		**1st**	**2nd**	**3rd**
237	1,420	506	0.0437	1.895	449	1,042	1,070	1,263
-1,342	265	555	0.0425	2.058	495	986	1,142	1,220
34	-277	557	0.0410	2.461	501	1,379	1,478	1,493
-1,083	-1,260	680	0.0430	1.889	622	927	1,050	1,222
1,298	759	683	0.0457	2.438	628	1,158	1,263	1,277
-788	1,324	797	0.0441	2.174	686	1,029	1,070	1,220
1,429	-810	811	0.0436	2.499	669	1,033	1,060	1,253
7	-1,764	909	0.0422	2.350	582	1,127	1,220	1,222
-1,548	-555	1,062	0.0420	1.591	659	927	958	986
1,694	-30	1,433	0.0458	1.713	587	902	1,033	1,157
581	1,537	1,482	0.0441	2.160	580	963	1,042	1,326
873	-1,375	1,516	0.0409	1.853	708	984	1,060	1,080
-1,566	419	1,664	0.0409	2.318	645	1,142	1,145	1,146
-819	-1,329	1,695	0.0426	1.969	773	979	1,050	1,080
-794	1,394	1,823	0.0407	2.501	623	1,029	1,254	1,424
91	38	1,898	0.0467	2.907	651	1,379	1,527	1,542
1,268	1,032	1,930	0.0436	2.102	606	963	1,248	1,277
-1,469	-669	2,011	0.0452	1.808	541	958	979	1,146
1,451	-639	2,052	0.0423	1.899	501	902	1,079	1,253
133	-1,611	2,119	0.0394	1.799	432	984	1,079	1,227

These data can be visualized for a subset of particles or for the full compact, as shown in Figure 6 and Figure 7. The particle configuration in this compact is typical for all compacts analyzed with three layers of particles at approximately the same height in the compact and ~6–8 particles within each layer. The consistency of the particle distribution in the XCT analyzed MiniFuel compacts reflects the decision to not select compacts which had no central particles (Figure 3).

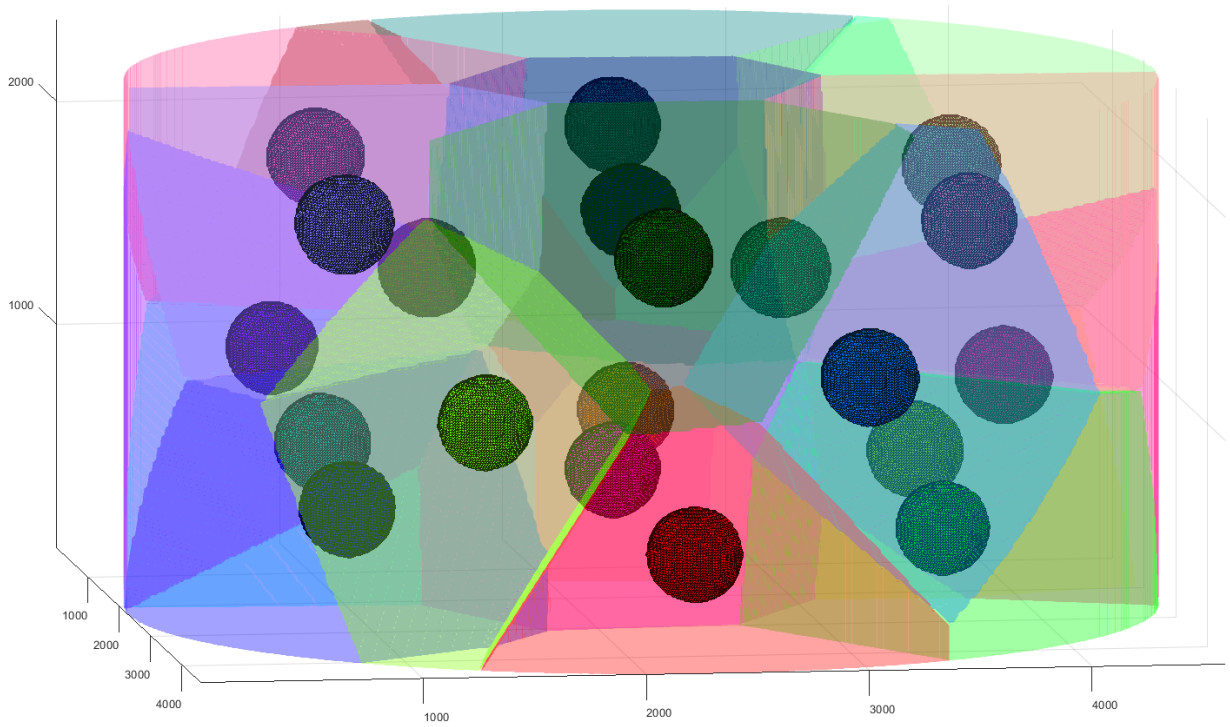

Figure 6. Side view of a 3D representation of an XCT image for a compact showing each particle and its associated region volume within the compact in a unique color.

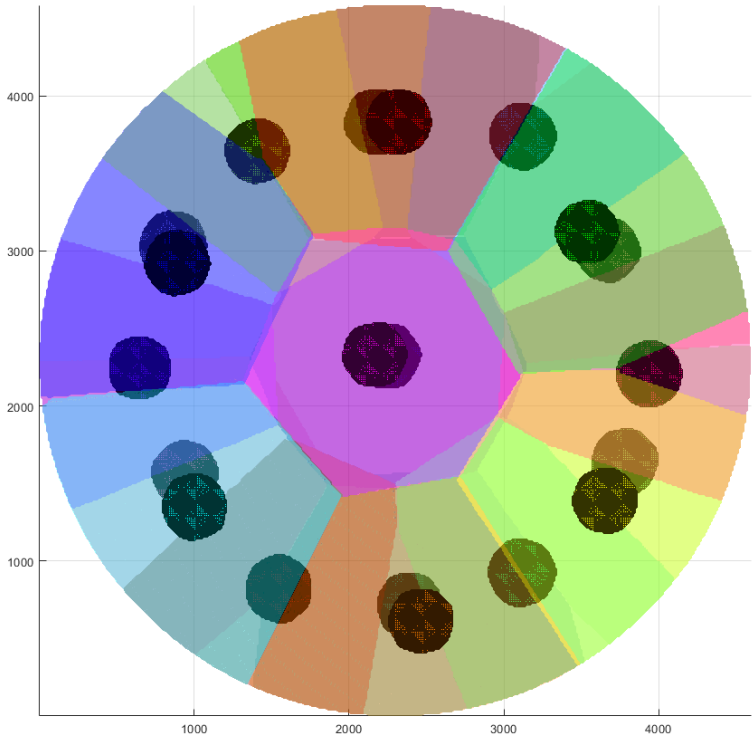

Figure 7. Top-down view of a 3D representation of an XCT image for a compact showing each particle and its associated region volume within the compact in a unique color.

3.2.3 Particle Failure Fraction Analysis

One primary metric for TRISO fuel performance is particle failure fraction. Modern TRISO particles have shown failure fractions better than ≤5.1E-5 at 95% confidence (Demkowicz et al. 2019). The planned irradiation intends to explore margin irradiation conditions and potentially push the operating envelope for fuel performance. Determining the as-fabricated defect fraction is important for interpreting failures observed in-pile relative to failure that might have been present from as-fabricated defects. The as-fabricated defect fraction for AGR-2 particles for UCO and UO_2 kernel variants measured multiple defect types, including uranium contamination fraction, defective SiC coating fraction, defective IPyC coating fraction, and defective OPyC coating fraction (Hunn et al. 2010a, Hunn et al. 2010b). The uranium contamination fraction and defective SiC coating fraction were equivalent to the defect fraction measured in this work because the values reflect the number of exposed kernel defects pre- and post-burn. The maximum reported failure fraction for the two AGR-2 fuel variants after compacting was ≤3.2E-5 at a 95% confidence level (Hunn et al. 2010a, Hunn et al. 2010b). The failure rate at a 95% confidence level was determined from a burn-back analysis of the MiniFuel compacts. MiniFuel compacts were subjected to a burn step similar to the burn step in the deconsolidation leach-burn-leach process (Hunn et al. 2013). MiniFuel compact clutches that contained no more than 120 particles each were subjected to a burn under forced air in a muffle furnace at 750°C for 48 h. The particle defect fraction was then determined by performing x-ray radiography analysis by using the same Zeiss Versa 520 XCT instrument. The radiographs were analyzed to look for defective particles. Defective particles with exposed kernel defects are indicated by fractured SiC, oxidized (i.e., swollen) kernels, and/or oxidized (i.e., missing) IPyC and buffer layers. Figure 8 provides an example of an exposed kernel defect after the burn step (Gerczak et al. 2016) in which a particle with a compromised SiC layer led to the burning out of the internal IPyC and buffer layers and the kernel swelling after exposure to forced air at 750°C.

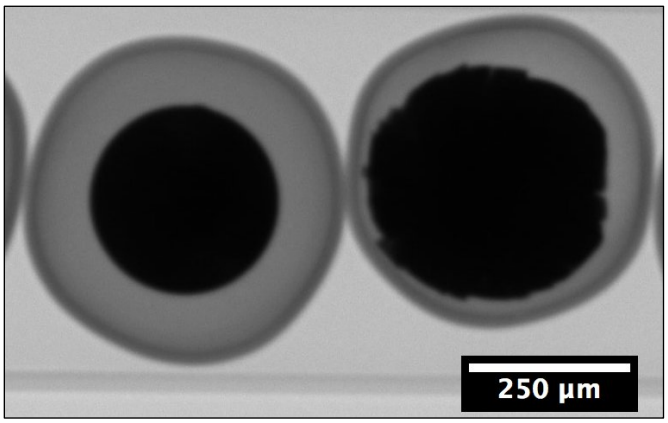

Figure 8. Example radiograph of an intact particle (left) and oxidized kernel and missing buffer/IPyC particle (right) after exposure to a burn stage (Gerczak et al. 2016).

Figure 9 shows an example radiograph of a burn test particle clutch. Each radiograph was analyzed for irregular or defect particles. A total of 1,360 particles were analyzed from the compacts selected for burn testing listed in Table 3–Table 6. No defective or failed particles were observed. The analysis reflected an as-fabricated defect fraction of ≤2.2E-3 at 95% confidence. This number serves as a baseline for establishing in-pile failures during irradiation. All radiographs used for defect analysis are shown in Appendix C.

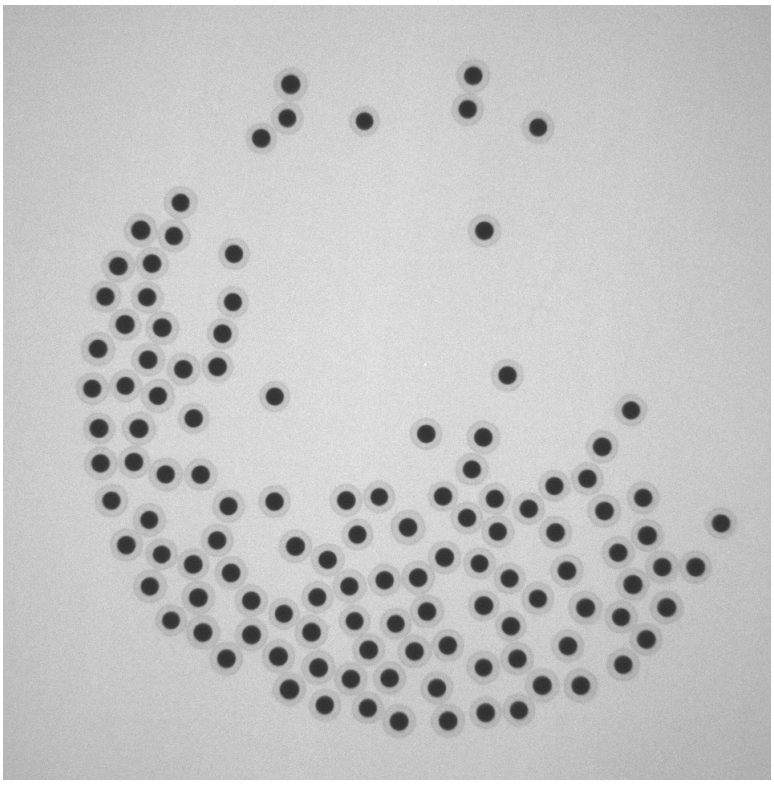

Figure 9. Example of radiography analysis of a 120 particle clutch after 750°C for 48 h under forced air from LEU09-M##E.

3.3 MATRIX IMPURITY ANALYSIS

Impurity content in the matrix was measured to support safety analysis and determine whether excess impurities were present. Excess impurities content is needed for safety analysis and is also needed to understand the potential for deleterious interactions with the TRISO particles in the MiniFuel compacts. Matrix samples were prepared and sent to Eurofins EAG Materials Science LLC for impurity analysis by glow discharge mass spectroscopy. The data were reported in concentration. The impurity analysis results are listed in Table 9 and are compared with specified limits, measured impurity, and contamination data from AGR-2 compacts (Collin 2014) data. The AGR-2 data were converted from the micrograms of each impurity outside the SiC/compact to parts-per-million weight by dividing by the average matrix material weight per compact. This is an estimate because it does not account for the OPyC layer weight. The data in Table 9 confirms that the impurity concentration was below the specified values and were on the order of or better than the measured impurity concentrations in the AGR-2 compacts.

Table 9. Select impurity data for matrix material from MiniFuel compacts.

	All values in parts-per-million by weight			
Impurity	**Specific range for AGR-2***	**Values for AGR-2 UCO compacts***	**Values for AGR-2 UO_2 compacts***	**This work**
Iron	≤8.3	1.34	0.71	0.46
Chromium	≤16.6	0.20	0.12	<1
Manganese	≤16.6	0.05	0.03	<0.05
Cobalt	≤16.6	0.37	0.03	<0.05
Nickel	≤16.6	0.32	0.15	0.17
Calcium	≤16.6	13.04	9.14	2.9
Aluminum	≤16.6	9.81	11.10	0.55
Titanium	-	0.93	0.86	0.89
Vanadium	-	5.67	4.01	1.4
Uranium**	-	1.59	1.57	<0.05
Molybdenum	-	-	-	<0.1

*Source data from Collin (2014), values converted to parts-per-million weight by dividing by the average matrix weight per compact.
**Contamination fraction reported as g U/g U in compact without exposed kernels.

4. SUMMARY

MiniFuel compacts were subjected to a series of preirradiation characterization techniques to provide relevant data for irradiation capsule design and HFIR safety analysis. The data were necessary for providing inputs to refine thermal models and HFIR safety calculations. The analysis confirmed that all compacts selected for archive or irradiation contained the necessary 20 particles. The measured densities were within the targeted ranges associated with the AGR-1 irradiation experiment. The density measurements allowed outlier compacts to be removed and compacts with a reasonable variance in density to be selected. Other down-selection criteria, such as having no particles in the compact center, were identified to support a more uniform comparison across compacts included in the planned irradiation. The XCT analysis provided unique insight into the kernel volume and particle positions within the individual compacts. These data will be critical for refining thermal modeling to better support temperature analysis and the interpretation of PIE results. Lastly, the as-fabricated defect analysis indicated that no particles failed during compact fabrication and provided a measure of the as-fabricated defects fraction at a 95% confidence level. The defect fraction will be critical when interpreting potential in-pile failures and the influence of irradiation conditions on TRISO particle performance.

5. REFERENCES

Brown, N.R., Betzler, B.R., Carbajo, J.J., Wysocki, A.J., Greenwood, M.S., Gentry, C., Qualls, A.L., 2017. "Preconceptual Design of a Fluoride High Temperature Salt-cooled Engineering Demonstration Reactor: Core Design and Safety Analysis," *Ann. Nucl. Energy*. 103, 49–59.

Bullock, R.E., Kaae, J.L., 1983. "Performance of Coated UO_2 Particles Gettered with ZrC," *J. Nucl. Mater.,* 115, 69–83.

BWXT, 2008a. *Industrial Fuel Fabrication and Development Lot G73AA-10-69308*. Data Certification Package.

BWXT, 2008b. *Industrial Fuel Fabrication and Development Lot G73I-14-69307*. Data Certification Package.

BWXT, 2008c. *Industrial Fuel Fabrication and Development Lot G73J-14-93071A, G73J-14-93073A, G73J-14-93074A.* Data Certification Package.

BWXT, 2009. *Industrial Fuel Fabrication and Development Lot G73H-10-93085B*. Data Certification Package.

Collin, B., 2014. *AGR-2 Irradiation Test Final As-Run Report*. INL/EXT-14-32277 Rev. 1. Idaho National Laboratory, Idaho Falls, Idaho. 2014.

Gallagher, R. C., Wallen, Z., Petrie, C. M., Gerczak., T. J., Le Coq, A., Smith, K., Harp, J., Linton, K., Collin, B., Latta, R., 2020. *Analysis and Design of High-Power TRISO Fuel Compact Irradiation in HFIR*. ORNL/TM-2020/1658, Oak Ridge National Laboratory, Oak Ridge, Tennessee.

Gerczak, T.J., Baldwin, C.A., Helmreich, G.W., Hunn, J.D., Montgomery, F.C., 2016. *Preparation of Simulated LBL Defects for Round Robin Experiments*. ORNL/TM-2015/722. Rev. 2.

Gerczak, T. J., Contescu, C., Lee, Y. J., Mee, R., Schumacher, A. T., Stempien, J., and Trammell, M. 2019. *Oxidation of Matrix Material in Helium with Varied Moisture Content*. ORNL/TM-2019/1341. Rev. 0.

Gerczak, T.J., Kercher, A., Schumacher, A.T., Helmreich, G.W., Trammell, M., 2020. *Fabrication of MiniFuel Compacts for High-Power Irradiation Testing of TRISO Fuel*. ORNL/TM-2020/1778. Rev. 0.

Helmreich, G.W., Hunn, J.D., McMurray, J.W., Brown, D.R., 2020a. "Enhanced Method for Analysis of Individual UCO Kernel Phase Fractions," *Nucl. Eng. Des*., 363, 110625.

Helmreich, G.W., Hunn, J.D., Brown, D.R., Blamer, B.J., 2020b. "New Method for Analysis of X-ray Computed Tomography Scans of TRISO Fuel Forms," *Nucl. Eng. Des*., 357, 110418.

Homan, F.J., Lindemer, T.B., Long Jr., E.L., Tiegs, T.N., Beatty, R.L., 1977. "Stoichiometric Effects on Performance of High Temperature Gas Cooled Reactor Fuels from the U C O System," *Nucl. Tech*. 35, 428–441.

Hunn, J.D., 2008. *Data Compilation for AGR-2 B&W UCO Coated Particle Batch G73J-14-93073A*. ORNL/TM-2008/134. Rev. 1.

Hunn, J.D., 2010. *Data Compilation for AGR-2 B&W UO_2 Coated Particle Batch G73H-10-93085B*. ORNL/TM-2010/255. Rev. 1.

Hunn, J. D., Montgomery, F. C., and Pappano, P. J., 2010a. *Data Compilation for AGR-2 B&W UCO Compact Lot LEU09-OP-Z*. ORNL/TM-2010/017. Rev. 1.

Hunn, J. D., Montgomery, F. C., and Pappano, P. J., 2010b. *Data Compilation for AGR-2 B&W UO_2 Compact Lot LEU11-OP-Z*. ORNL/TM-2010/055. Rev. 1.

Hunn, J. D., Savage, T. W., Silva, G. W. C., 2010c. *AGR-2 Fuel Compact Pre-Irradiation Characterization Summary Report*. ORNL/TM-2010/226. Rev. 1.

Hunn, J. D., Trammell, M. P., and Montgomery, F. C., 2011. *Data Compilation for AGR-3/4 Matrix Ring Blank Lot RDKRS*. ORNL/TM-2011/127. Rev. 1.

Hunn, J .D., Savage, T. W., Silva, C. M., 2012. *AGR-1 Fuel Compact Pre-Irradiation Characterization Summary Report*. ORNL/TM-2012/295. Rev. 0.

Hunn, J. D., Morris, R. N., Baldwin, C. A., Montgomery, F. C., Silva, G. W. C., and Gerczak, T. J., 2013. *AGR-1 Irradiated Compact 4-4-2 PIE Report : Evaluation of As-Irradiated Fuel Performance with Leach Burn Leach , IMGA , Materialography, and X-ray Tomography.* ORNL/TM-2013/236, Oak Ridge National Laboratory, Oak Ridge, Tennessee.

Hunn, J. D., Lowden, R. A., Miller., J. H., Jolly., B. C., Trammell, M. P., Kercher, A. K., Montgomery., F. C., Silva., C. M., 2014. "Fabrication and Characterization of Driver-Fuel Particles, Designed-to-Fail Fuel Particles, and Fuel Compacts for the US AGR-3/4 Irradiation Test." *Nucl. Eng. Des*. 271: 123–130.

Latta, R., Collin, B., Hackett, M., Brown, N. R., Hunn, J. D., Petrie, C. M., Gerczak., T. J., and Helmreich., G. W., 2019. "High Power Irradiation Testing of TRISO Particles in Miniature Fuel Specimens in HFIR," *ANS Transactions*, 121, 1: 641–643.

Maki, J.T., Petti, D.A., Knudson, Miller, G.K., 2007. "The Challenge Associated with High Burnup, High Temperature and Accelerated Irradiation for TRISO Coated Particle Fuel," *J. Nucl. Mater*., 371, 270–280.

McMurray, J.W., Lindemer, T.B., Brown, N.R., Reif, T.J., Morris, R.N., 2017. "Determining the Minimum Required Uranium Carbide Content for HTGR UCO Fuel Kernels," *Ann. Nucl. Energy*., 104, 237–424.

Pappano, P. J., Burchell, T. D., Hunn, J. D., and Trammell, M. P., 2008. "A Novel Approach to Fabricating Fuel Compacts for the Next Generation Nuclear Plant (NGNP)." *J. Nucl. Mater.* 381, 1–2: 25–38.

Pappano, P. J. and Hunn, J. D., 2008. "Update on Overcoating and Compacting Activities for Coated Particles with 425 μm Kernels" *Proceedings of the 4th International Topical Meeting on High Temperature Reactor Technology*. HTR2008 September 28–October 1, 2008, Washington, DC.

Petrie, C. M., Burns, J. R., Raftery, A. M., Nelson, A.T ., and Terrani, K. A., 2019. "Separate Effects Irradiation Testing of Miniature Fuel Specimens," *J. Nucl. Mater.* 526, 151783.

Petti, D., Maki, J., Hunn, J., Pappano, P., Barnes, C., Saurwein, J., Nagley, S., Kendall, J., and Hobbins, R., 2010. "The DOE Advanced Gas Reactor Fuel Development and Qualification Program," *JOM-US*. 61: 62–66.

Seibert R.L., Terrani, K.A., Kiggans, J.O., McMurray, J.W., Jolly, B.C., Petrie, C.M., and Nelson, A.T., 2019. *Fabrication and Irradiation Test Plan for Fully Ceramic Microencapsulated Fuels.* ORNL/TM-2019/1088, Oak Ridge National Laboratory, Oak Ridge, Tennessee.

Terrani, K.A., Snead, L.L., Gehin, J.C., 2012. "Microencapsulated fuel technology for commercial light water and advanced reactor application," *J. Nucl. Mater.,* 427. 209–224.

APPENDIX A.

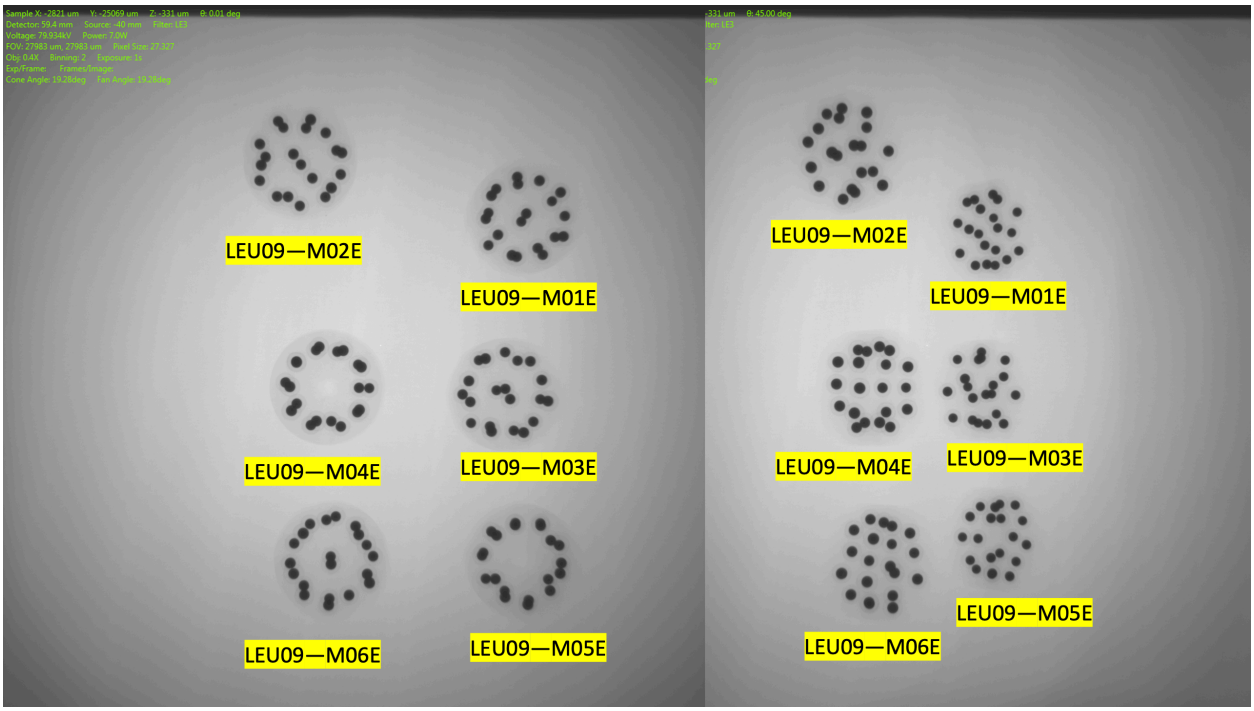

Figure A-1. Radiography sets of LEU09-M01E–LEU09-M06E; axial image orientation (left) and 45° tilt from the axial direction (right).

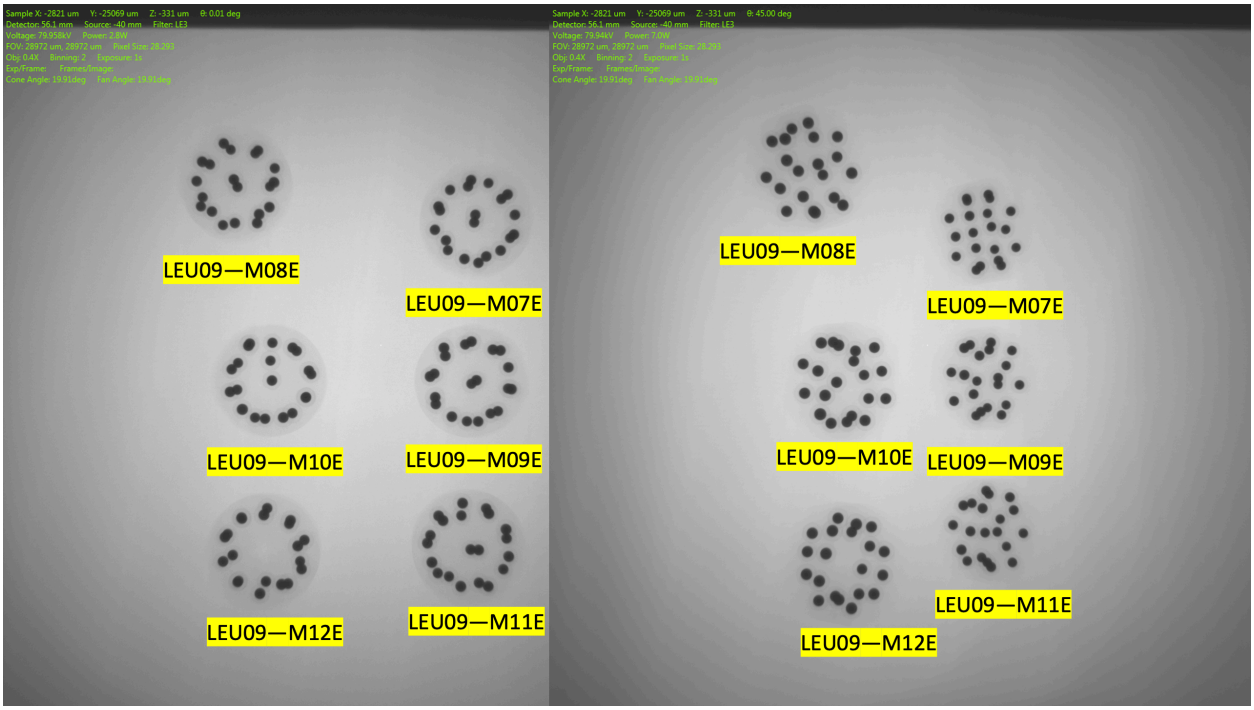

Figure A-2. Radiography sets of LEU09-M07E–LEU09-M12E; axial image orientation (left) and 45° tilt from the axial direction (right).

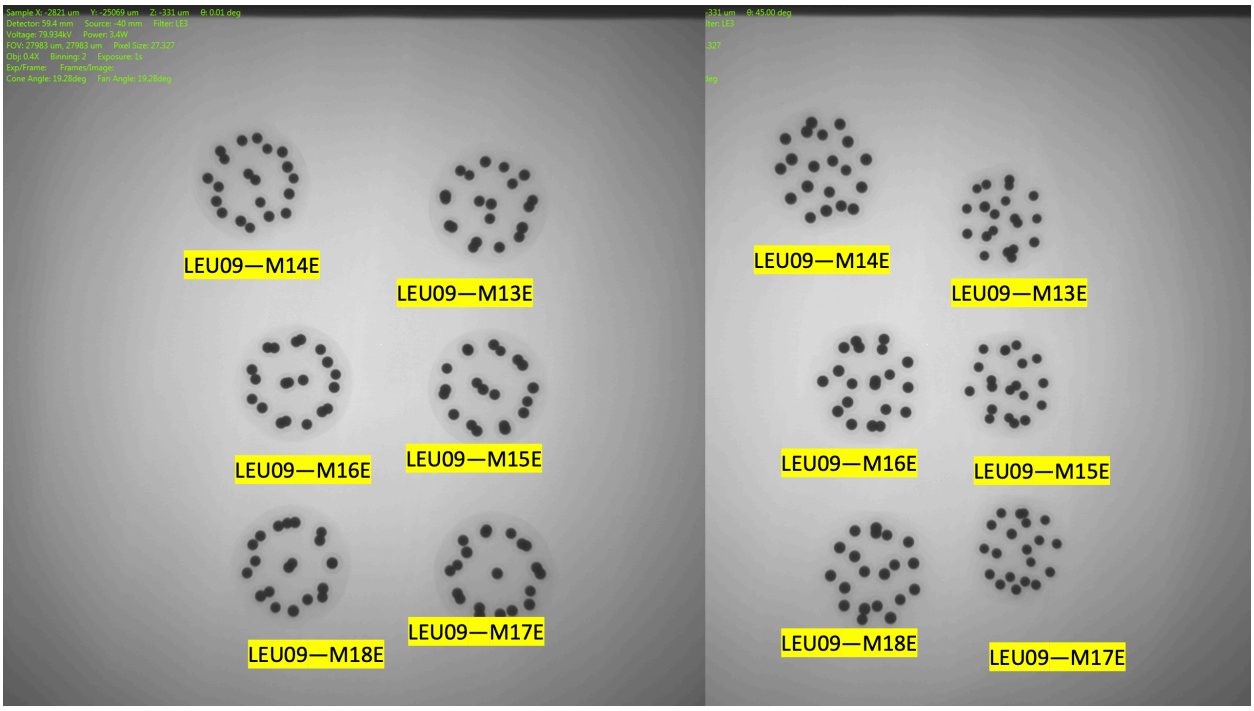

Figure A-3. Radiography sets of LEU09-M13E–LEU09-M18E; axial image orientation (left) and 45° tilt from the axial direction (right).

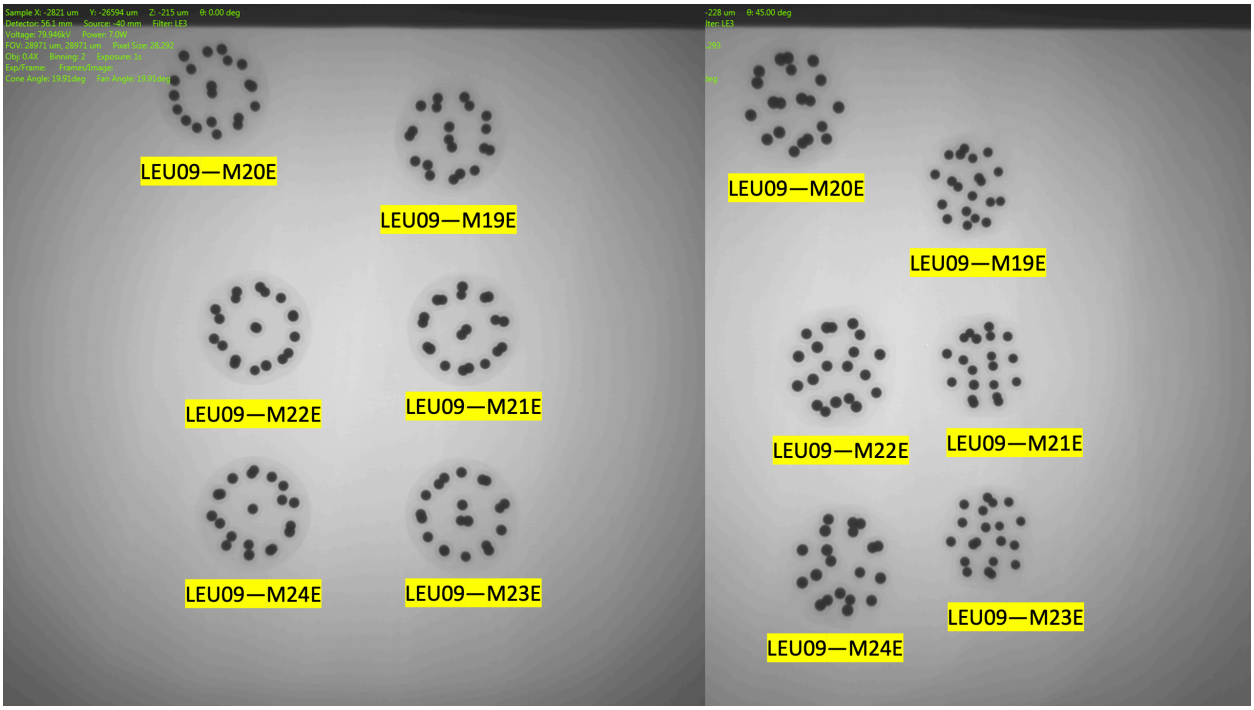

Figure A-4. Radiography sets of LEU09-M19E–LEU09-M24E; axial image orientation (left) and 45° tilt from the axial direction (right).

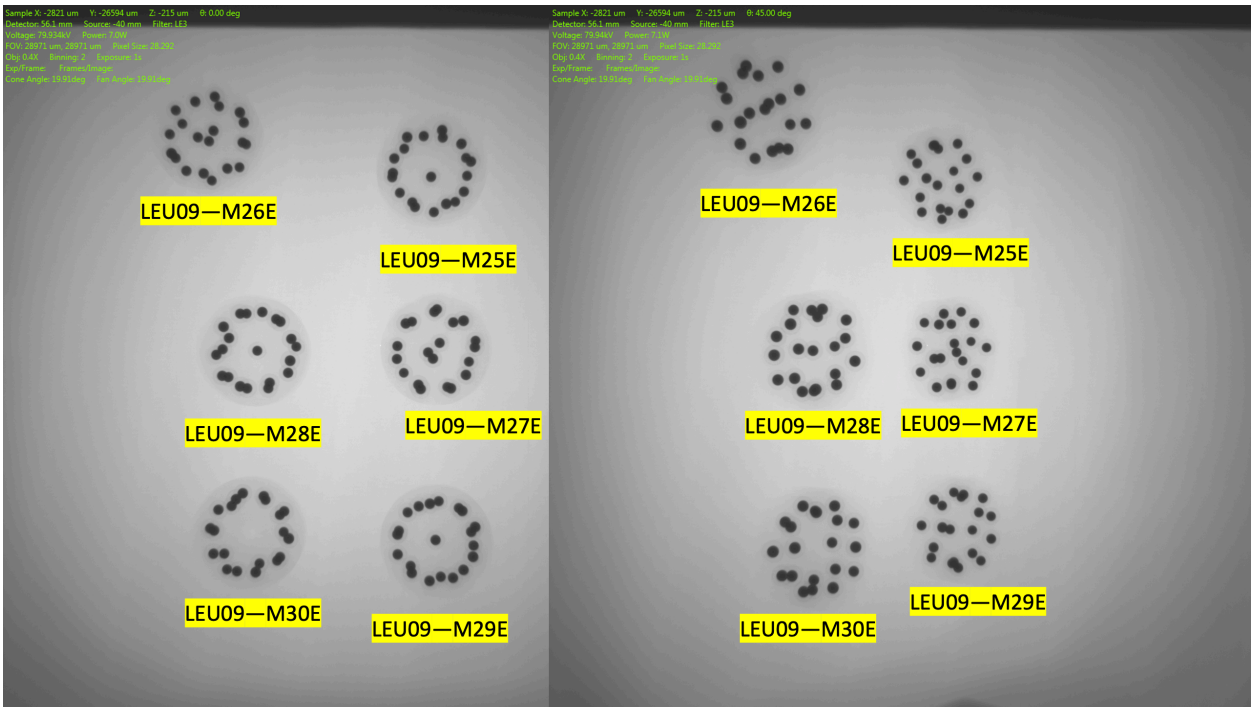

Figure A-5. Radiography sets of LEU09-M25E–LEU09-M30E; axial image orientation (left) and 45° tilt from the axial direction (right).

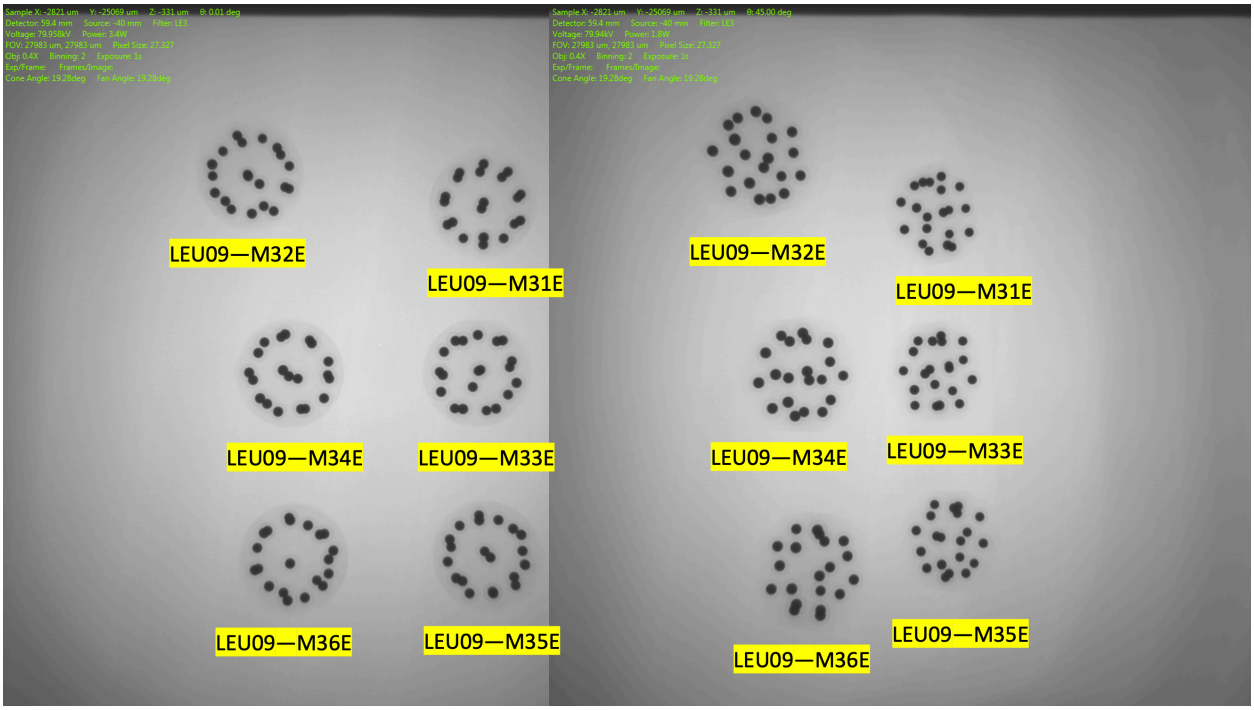

Figure A-6. Radiography sets of LEU09-M31E–LEU09-M36E; axial image orientation (left) and 45° tilt from the axial direction (right).

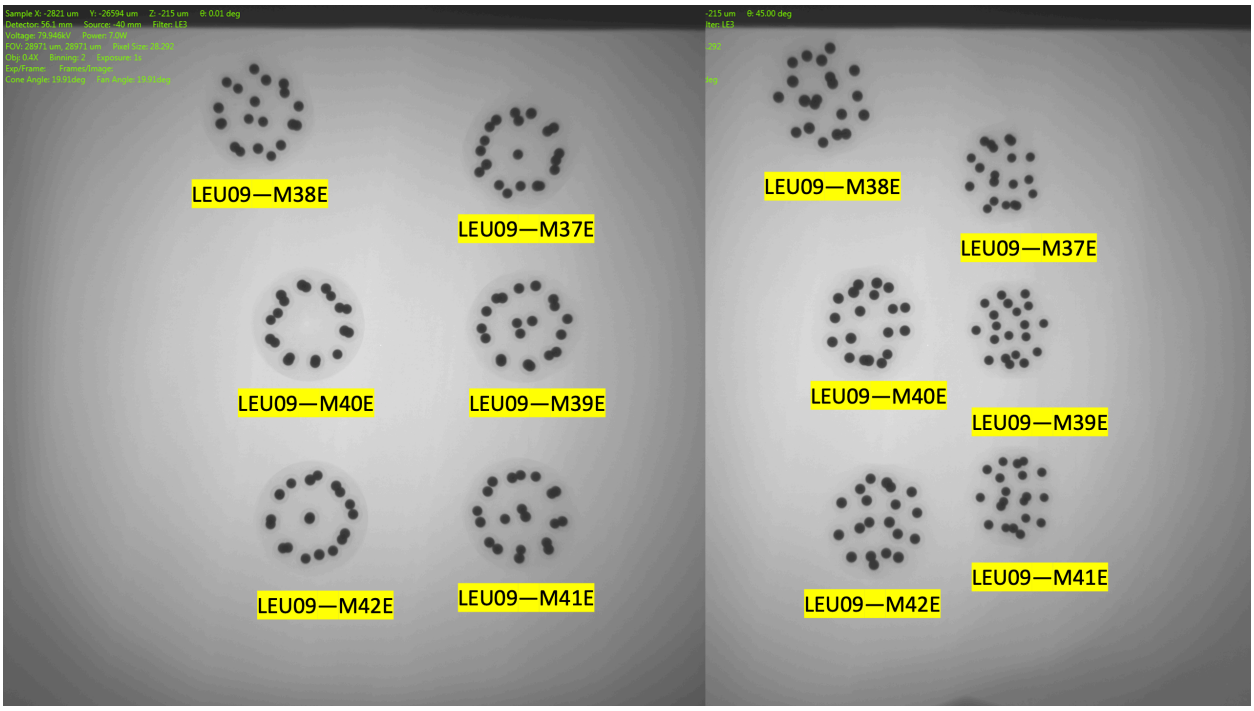

Figure A-7. Radiography sets of LEU09-M37E–LEU09-M42E; axial image orientation (left) and 45° tilt from the axial direction (right).

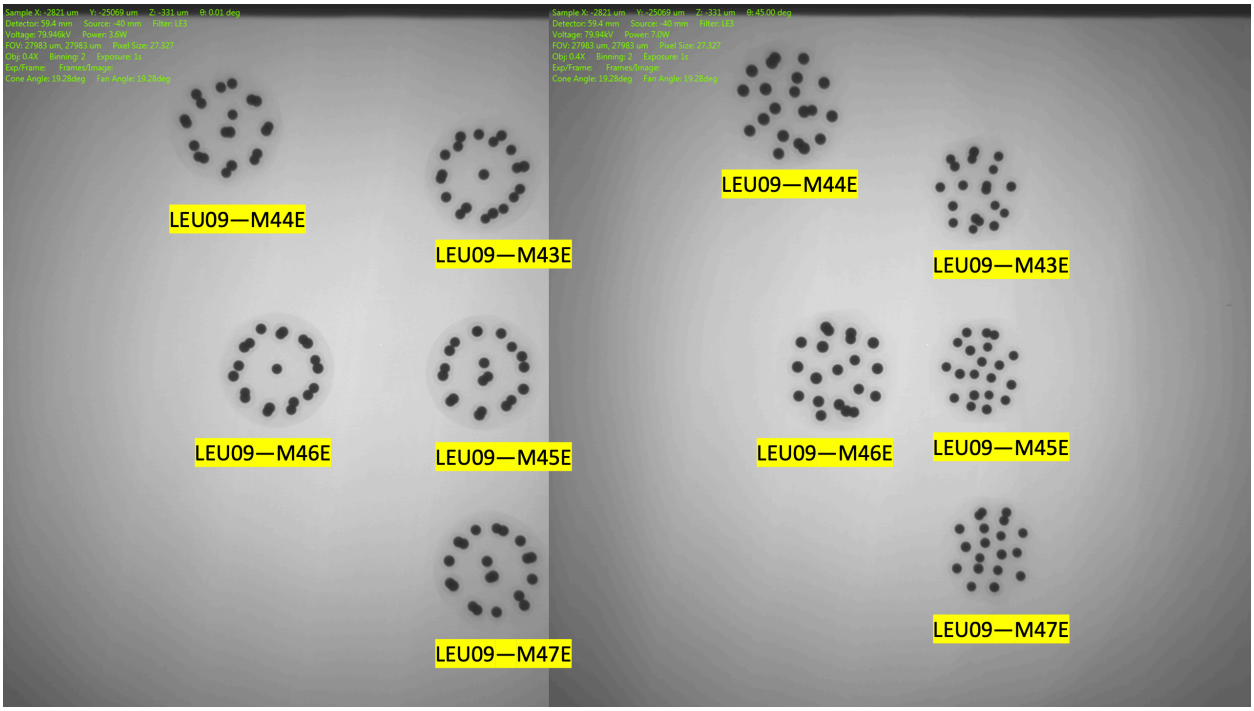

Figure A-8. Radiography sets of LEU09-M43E–LEU09-M47E; axial image orientation (left) and 45° tilt from the axial direction (right).

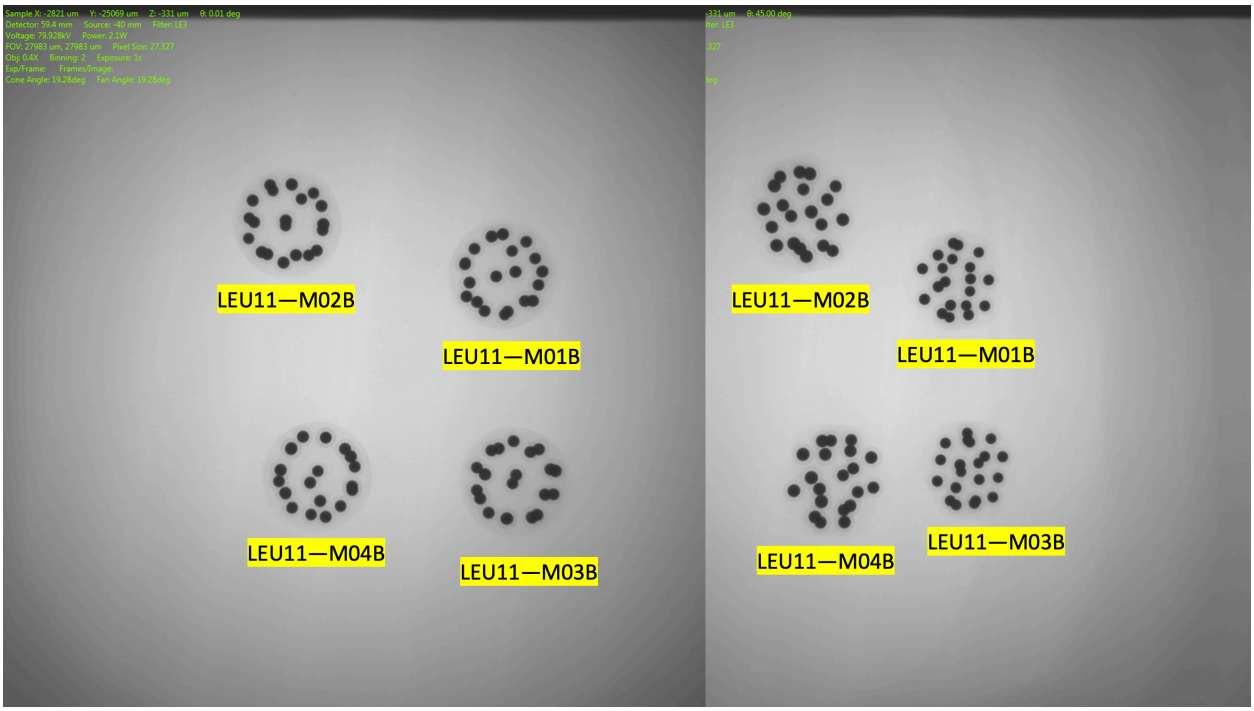

Figure A-9. Radiography sets of LEU11-M01B–LEU11-M04B; axial image orientation (left) and 45° tilt from the axial direction (right).

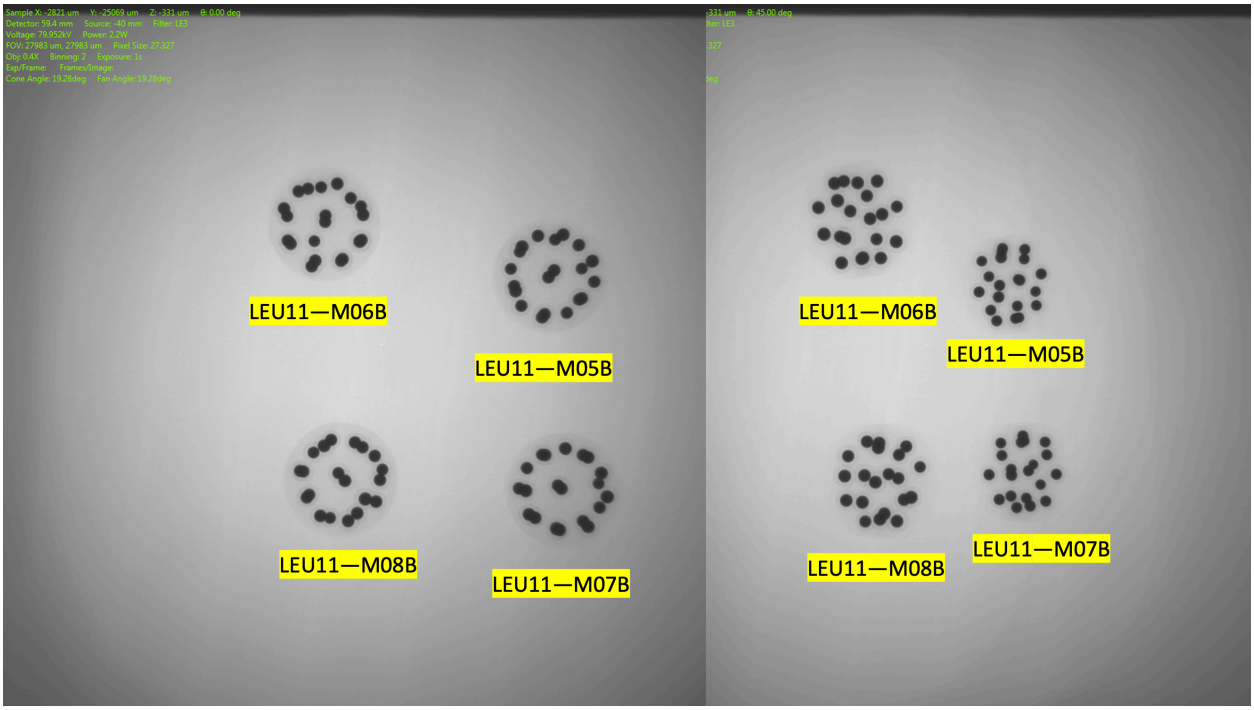

Figure A-10. Radiography sets of LEU11-M05B–LEU11-M08B; axial image orientation (left) and 45° tilt from the axial direction (right).

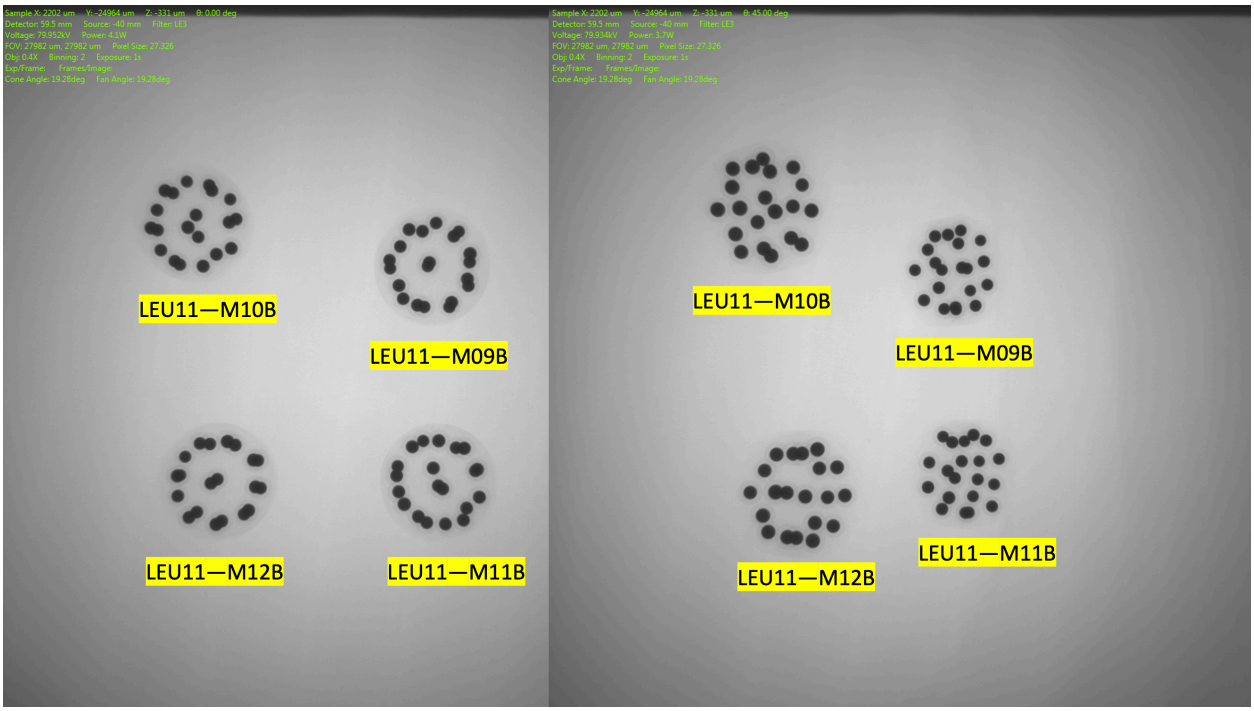

Figure A-11. Radiography sets of LEU11-M09B–LEU11-M12B; axial image orientation (left) and 45° tilt from the axial direction (right).

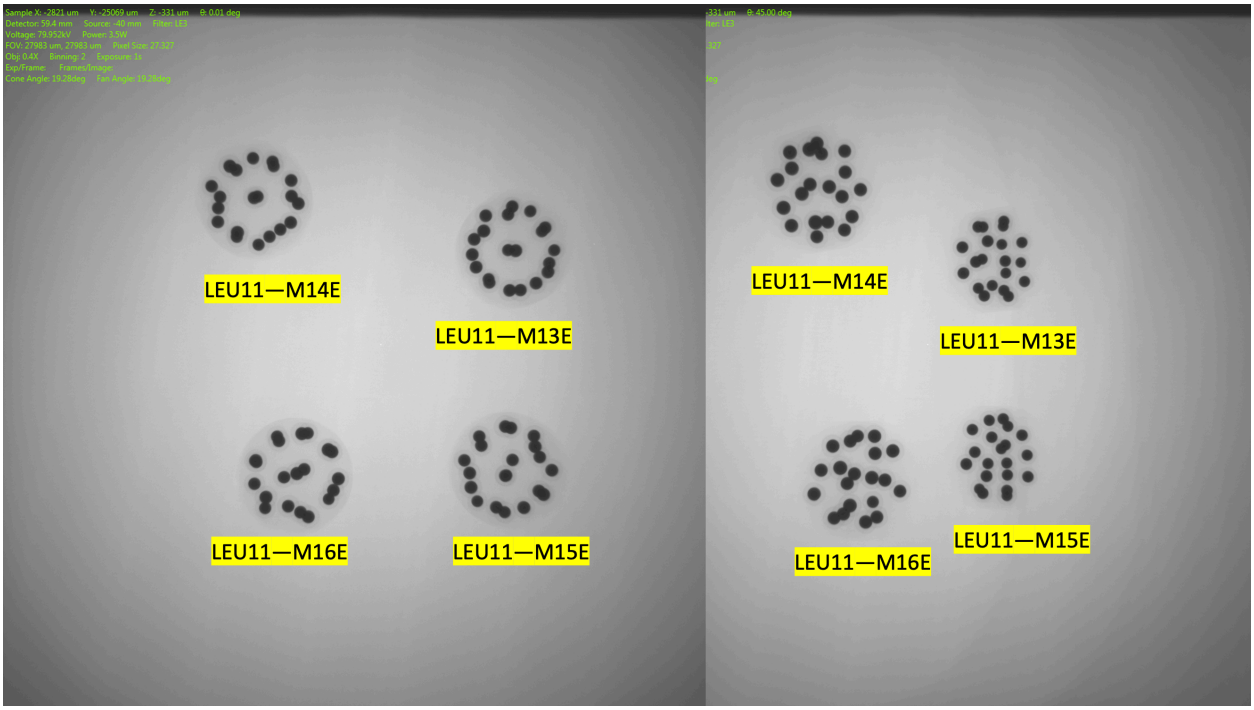

Figure A-12. Radiography sets of LEU11-M13B–LEU11-M16B; axial image orientation (left) and 45° tilt from the axial direction (right).

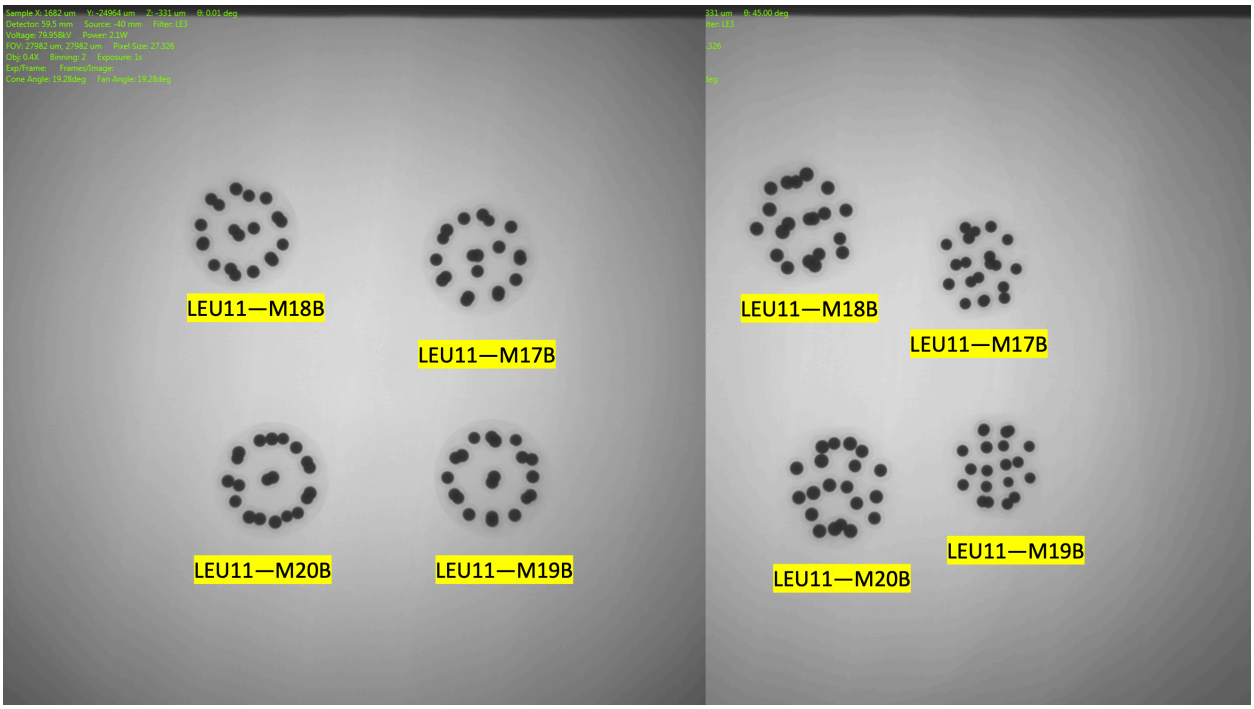

Figure A-13. Radiography sets of LEU11-M17B–LEU11-M20B; axial image orientation (left) and 45° tilt from the axial direction (right).

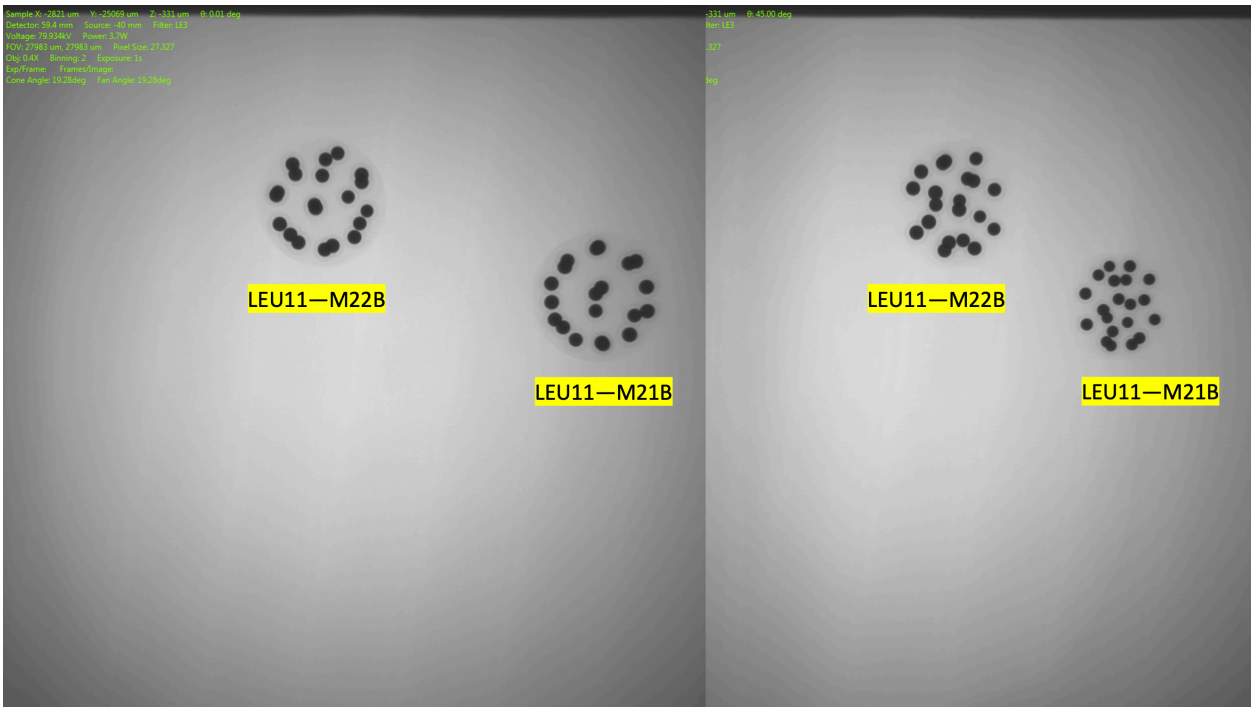

Figure A-14. Radiography sets of LEU11-M21B–LEU11-M22B; axial image orientation (left) and 45° tilt from the axial direction (right).

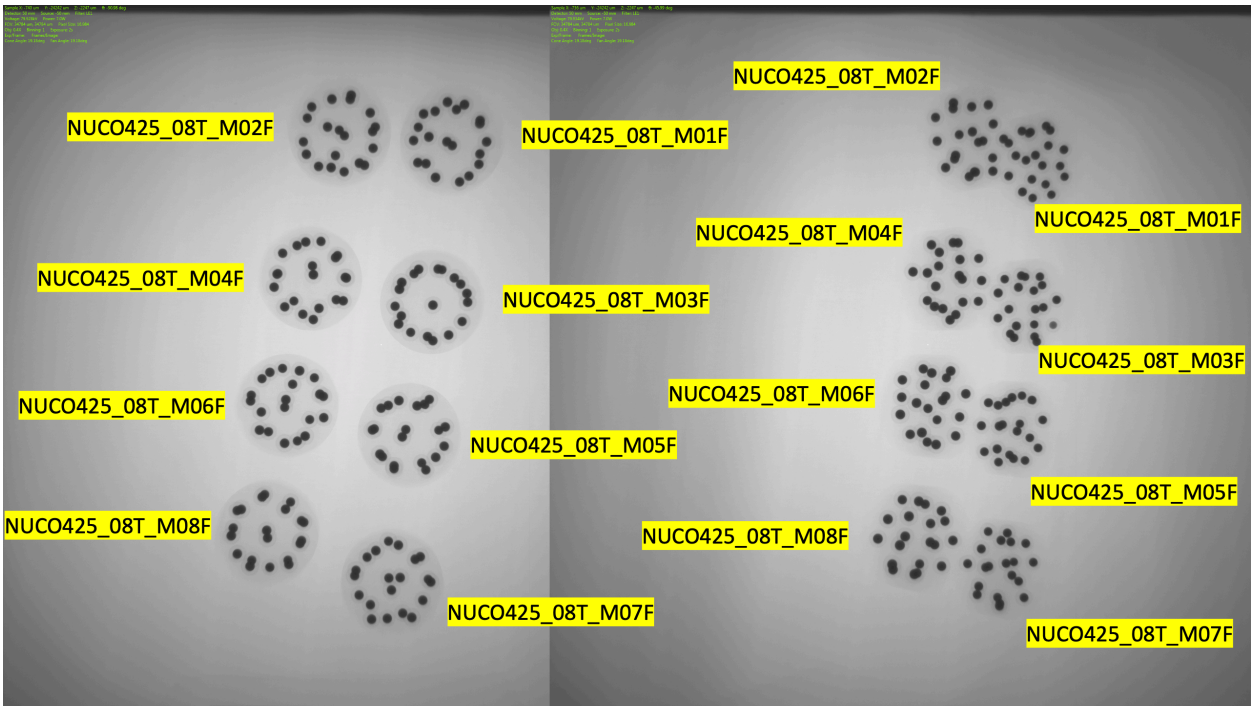

Figure A-15. Radiography sets of NUCO425-08T-M01F– NUCO425-08T-M08F; axial image orientation (left) and 45° tilt from the axial direction (right).

APPENDIX B.

Table B-1. XCT data for particles in compact NUCO-M01F.

Centroid (μm)			Volume (mm^3)		Surface distance (μm)	Nearest neighbor (μm)		
x	***y***	***z***	**Kernel**	**Region**		**1st**	**2nd**	**3rd**
237	1,420	506	0.0437	1.895	449	1,042	1,070	1,263
-1,342	265	555	0.0425	2.058	495	986	1,142	1,220
34	-277	557	0.0410	2.461	501	1,379	1,478	1,493
-1,083	-1,260	680	0.0430	1.889	622	927	1,050	1,222
1,298	759	683	0.0457	2.438	628	1,158	1,263	1,277
-788	1,324	797	0.0441	2.174	686	1,029	1,070	1,220
1,429	-810	811	0.0436	2.499	669	1,033	1,060	1,253
7	-1,764	909	0.0422	2.350	582	1,127	1,220	1,222
-1,548	-555	1,062	0.0420	1.591	659	927	958	986
1,694	-30	1,433	0.0458	1.713	587	902	1,033	1,157
581	1,537	1,482	0.0441	2.160	580	963	1,042	1,326
873	-1,375	1,516	0.0409	1.853	708	984	1,060	1,080
-1,566	419	1,664	0.0409	2.318	645	1,142	1,145	1,146
-819	-1,329	1,695	0.0426	1.969	773	979	1,050	1,080
-794	1,394	1,823	0.0407	2.501	623	1,029	1,254	1,424
91	38	1,898	0.0467	2.907	651	1,379	1,527	1,542
1,268	1,032	1,930	0.0436	2.102	606	963	1,248	1,277
-1,469	-669	2,011	0.0452	1.808	541	958	979	1,146
1,451	-639	2,052	0.0423	1.899	501	902	1,079	1,253
133	-1,611	2,119	0.0394	1.799	432	984	1,079	1,227

Table B-2. XCT data for particles in compact NUCO-M02F.

Centroid (μm)			Volume (mm^3)		Surface distance (μm)	Nearest neighbor (μm)		
x	***y***	***z***	**Kernel**	**Region**		**1st**	**2nd**	**3rd**
-1,507	-344	785	0.0387	2.011	476	940	1,151	1,359
-848	-1,699	778	0.0379	2.169	476	1,035	1,284	1,397
-50	-194	821	0.0388	2.117	510	851	1,378	1,465
-753	1,162	834	0.0373	1.849	532	936	1,145	1,147
1,197	894	862	0.0357	2.153	555	934	1,228	1,424
1,067	-1,569	893	0.0346	1.986	589	1,008	1104	1,180
1,618	-623	1,040	0.0396	2.356	638	1,104	1,194	1,328
78	1,206	1,262	0.0393	2.028	770	936	1,060	1,137
-1,419	394	1,361	0.0398	2.185	695	940	1,145	1165
260	-1,907	1,393	0.0410	2.035	682	1,008	1,075	1,198
381	-477	1,498	0.0437	1.590	1,178	851	886	1,326
-1,359	-1,207	1,532	0.0430	1.777	663	900	1,035	1,151
1,439	538	1,691	0.0452	1.847	610	934	1,035	1,113
-803	1,166	1,980	0.0402	2.495	603	1,137	1,147	1,165
1,181	-1,540	2,067	0.0431	2.228	591	1,180	1,198	1,229
-1,740	-618	2,096	0.0419	2.109	520	900	1,292	1,359
-530	-1,904	2,123	0.0428	2.218	555	1,075	1,234	1,397
661	1,189	2,148	0.0442	2.179	521	1,060	1,113	1,424
-199	-445	2,167	0.0415	2.283	510	886	1,378	1,497
1,500	-361	2,199	0.0436	1.980	476	1,035	1,194	1,229

Table B-3. XCT data for particles in compact NUCO-M04F.

Centroid (μm)			Volume (mm^3)		Surface distance (μm)	Nearest neighbor (μm)		
x	***y***	***z***	**Kernel**	**Region**		**1st**	**2nd**	**3rd**
1,211	-1,153	782	0.0384	1.906	453	872	1,035	1,385
1,052	700	805	0.0364	1.980	476	906	961	1,309
-1,139	-1,346	822	0.0402	2.015	498	881	1,165	1,345
70	-1,934	859	0.0376	2.425	532	1,214	1,296	1,345
-712	1,159	918	0.0390	2.010	589	1,082	1,171	1,222
-45	-6	911	0.0380	2.310	578	1,103	1,309	1,322
-1,592	-324	1,152	0.0414	2.226	698	877	1,165	1,193
1,689	-589	1,245	0.0394	2.006	585	872	888	1,368
448	1,157	1,302	0.0446	1.852	728	906	921	1,043
-1,481	526	1,340	0.0412	1.729	575	877	944	1,082
968	-1,683	1,637	0.0446	2.020	637	839	1,035	1,214
-1,214	-1,645	1,647	0.0415	1.946	506	837	881	1,460
1,308	751	1,730	0.0429	1.884	591	839	961	1,043
-195	-261	1,975	0.0428	2.328	702	1,103	1,191	1,343
-617	1,092	2,084	0.0441	2.173	589	1,171	1,231	1,273
1,463	-517	2,100	0.0410	2.520	578	888	1,330	1,349
276	-1,677	2,113	0.0396	2.482	555	839	1,296	1,466
699	1,104	2,186	0.0424	1.763	487	839	921	1,320
-1,438	185	2,219	0.0460	1.858	453	944	1,193	1,231
-1,047	-1,056	2,218	0.0471	1.871	453	837	1,191	1,302

Table B-4. XCT data for particles in compact NUCO-M05F.

Centroid (μm)			Volume (mm^3)		Surface distance (μm)	Nearest neighbor (μm)		
x	***y***	***z***	**Kernel**	**Region**		**1st**	**2nd**	**3rd**
968	1,121	503	0.0421	1.881	443	1,079	1,145	1,265
-525	1,348	522	0.0401	1.865	466	1,043	1,049	1,335
-1,490	-320	641	0.0401	2.275	582	882	1,076	1,222
1,114	-1,280	713	0.0423	2.198	628	843	1,058	1,545
1,594	188	724	0.0410	2.210	660	1,030	1,145	1,248
-1,352	742	742	0.0446	1.205	685	293	1,049	1,076
-578	-1,625	755	0.0400	2.267	612	872	1,031	1,512
-43	112	815	0.0452	2.814	760	1,270	1,359	1,454
-1,575	552	737	0.0002	0.977	582	293	882	1,223
1,380	-677	1,239	0.0434	1.641	762	843	859	1,030
321	-1,732	1,248	0.0431	1.820	575	909	1,031	1,058
513	1,621	1,343	0.0430	1.844	518	973	1,079	1,143
-1,031	-1,522	1,493	0.0441	1.727	491	870	872	1,353
-405	1,376	1,558	0.0468	2.003	781	973	994	1,043
1,363	942	1,692	0.0441	2.288	579	1,139	1,143	1,248
-1,701	-68	1,818	0.0453	1.992	573	1,072	1,173	1,222
-1,217	887	1,856	0.0453	2.150	691	994	1,072	1,131
320	561	1,946	0.0434	2.255	599	1,139	1,158	1,234
190	-1,232	1,996	0.0399	2.402	547	909	1,173	1,353
1,474	-551	2,084	0.0441	2.231	461	859	1,456	1,547

Table B-5. XCT data for particles in compact NUCO-M06F.

Centroid (μm)			Volume (mm^3)		Surface distance (μm)	Nearest neighbor (μm)		
x	***y***	***z***	**Kernel**	**Region**		**1st**	**2nd**	**3rd**
452	1,587	507	0.0444	1.627	449	869	1,065	1,342
-1,218	871	521	0.0445	1.963	466	1,074	1,115	1,214
1628	410	605	0.0417	2.133	547	1,073	1,299	1,333
-1,254	-818	644	0.0402	2.079	587	938	953	1,134
162	-1,660	700	0.0427	2.043	645	977	1,005	1,254
156	-93	717	0.0423	3.215	656	1,471	1,560	1,567
1,263	-1,060	719	0.0306	2.203	662	1,065	1,254	1,274
-351	1,500	829	0.0419	1.767	683	869	1,065	1,115
-1,557	-6	1,039	0.0433	1.860	727	921	953	1,074
-686	-1,366	1,152	0.0430	1.631	814	899	924	938
946	1,246	1,387	0.0407	1.748	669	893	955	1,065
1,606	-314	1,396	0.0454	1.791	665	1,041	1,063	1,065
500	-1,583	1,613	0.0447	1.712	687	954	960	977
-1,057	1,109	1,701	0.0505	2.187	707	976	1,188	1,200
-1,254	-975	1,767	0.0395	2.126	656	924	1,071	1,134
98	1,422	1,791	0.0449	2.384	633	955	1,065	1,200
1,357	610	1,859	0.0462	2.281	564	893	1,063	1,299
-1,509	271	1,916	0.0426	2.006	507	921	976	1,280
-383	-1,560	1,976	0.0457	1.744	449	899	954	1,071
1,222	-1,077	1,992	0.0422	1.911	432	960	1,041	1,274

Table B-6. XCT data for particles in compact NUCO-M07F.

Centroid (μm)			Volume (mm^3)		Surface distance (μm)	Nearest neighbor (μm)		
x	***y***	***z***	**Kernel**	**Region**		**1st**	**2nd**	**3rd**
-1,122	765	775	0.0388	2.314	442	959	1,145	1,607
-1,441	-947	772	0.0357	1.655	442	877	997	1,172
407	12	851	0.0369	2.137	521	844	1,326	1,330
-125	-2,026	857	0.0382	1.787	532	1,102	1,102	1,247
1,060	-1,637	889	0.0388	1.898	566	980	1,247	1,257
1,758	-601	1,034	0.0377	2.366	503	1,209	1,211	1,257
-102	-598	1,135	0.0362	1.870	804	844	1,080	1,331
-1,573	-196	1,205	0.0404	1.967	711	877	983	1,145
598	1,232	1,346	0.0402	3.090	598	924	1,278	1330
-1,007	-1,614	1,373	0.0413	1.693	661	997	1,024	1,041
578	-1,910	1,698	0.0434	1.710	612	980	1,064	1,068
-1,113	868	1,729	0.0453	2.320	646	913	959	1,271
-1,387	-826	1,937	0.0436	2.730	736	983	1,041	1,172
1,585	160	1,960	0.0408	2.450	627	1,158	1,211	1,279
-92	-71	2,077	0.0399	2.101	600	1,080	1,130	1,326
1,464	-1,106	2,092	0.0438	1.876	578	920	1,209	1,260
-424	1,332	2,106	0.0470	1.948	563	913	1,278	1,387
-401	-1,982	2,111	0.0472	1.929	566	1,024	1,064	1,285
939	1,092	2,194	0.0416	1.731	476	924	1,158	1,387
562	-981	2,223	0.0442	1.508	453	920	1,068	1,130

Table B-7. XCT data for particles in compact LEU09-M01E.

Centroid (μm)			Volume (mm^3)		Surface distance (μm)	Nearest neighbor (μm)		
x	***y***	***z***	**Kernel**	**Region**		**1st**	**2nd**	**3rd**
674	1,132	787	0.0446	2.054	464	1,075	1,090	1,355
-1,346	-264	785	0.0429	1.998	453	1,076	1,103	1,180
-1,086	887	793	0.0453	1.933	464	1,069	1,180	1,274
-507	-1,736	927	0.0433	2.293	600	1,000	1,083	1,332
1,086	-1,662	974	0.0455	2.215	598	1,018	1,221	1,328
120	-379	998	0.0430	2.563	668	1,129	1,485	1,497
1,629	-450	997	0.0454	2.372	668	1,150	1,207	1,328
-1,402	-1,227	1261	0.0484	2.107	647	1,045	1,076	1,083
-249	1,307	1309	0.0441	1.904	635	1,069	1,075	1,115
1,371	586	1423	0.0494	2.151	644	1,063	1,090	1,150
271	-1,921	1528	0.0461	1.784	702	969	1,000	1,018
-1,606	217	1743	0.0456	2.037	605	1,078	1,078	1,103
1,441	-1,098	1998	0.0440	2.107	669	1,029	1,075	1,207
-968	1,006	2107	0.0454	2.356	647	1,078	1,115	1,324
-65	-284	2107	0.0417	2.579	679	1,129	1,411	1,466
524	1,196	2132	0.0414	2.619	657	1,135	1,262	1,355
-1,452	-752	2190	0.0477	2.203	600	1,045	1,078	1,286
-756	-1,833	2232	0.0428	2.203	555	1,248	1,286	1,315
1,497	-57	2259	0.0474	2.243	521	1,063	1,075	1,329
572	-1,518	2356	0.0416	1.940	430	969	1,029	1,370

Table B-8. XCT data for particles in compact LEU09-M07E.

Centroid (μm)			Volume (mm^3)		Surface distance (μm)	Nearest neighbor (μm)		
x	***y***	***z***	**Kernel**	**Region**		**1st**	**2nd**	**3rd**
24	1,188	794	0.0441	2.074	453	1,100	1,112	1,341
1,237	477	797	0.0411	2.206	453	1,067	1,145	1,372
-1,405	279	905	0.0441	2.093	566	962	1,004	1,297
1,356	-1,255	921	0.0441	2.151	577	969	1,039	1,337
-132	-315	980	0.0420	2.591	645	1,157	1,407	1,521
-1,296	-1,294	996	0.0453	2.455	657	1,034	1,107	1,327
168	-2,031	1,015	0.0432	2.352	612	981	1,162	1,300
1,640	-438	1,357	0.0464	1.918	657	969	1,052	1,145
-888	998	1,378	0.0428	1.976	688	1,004	1,095	1,100
-1,650	-399	1,542	0.0402	1.721	650	962	1,050	1,067
823	1,094	1,562	0.0459	2.018	639	1,067	1,092	1,098
819	-1,720	1,680	0.0487	1.751	713	981	983	1,039
-750	-1,824	1,696	0.0467	1.897	658	1,034	1,048	1,134
-114	1,189	2,128	0.0462	2.461	600	1,095	1,098	1,341
-51	-323	2,134	0.0440	2.545	600	1,157	1,514	1,520
1,372	361	2,158	0.0422	2.438	566	1,092	1,163	1,372
-1,433	394	2,196	0.0480	2.213	532	1,050	1,153	1,297
1,483	-1,005	2,228	0.0474	2.126	498	1,052	1,119	1,337
-1,356	-1,083	2,306	0.0455	2.031	419	1,067	1,134	1,327
93	-1,930	2,309	0.0438	1.880	419	983	1,048	1,300

Table B-9. XCT data for particles in compact LEU09-M14E.

Centroid (μm)			Volume (mm^3)		Surface distance (μm)	Nearest neighbor (μm)		
x	***y***	***z***	**Kernel**	**Region**		**1st**	**2nd**	**3rd**
38	1,048	791	0.0443	2.001	464	1,056	1,141	1,167
1,150	802	862	0.0431	2.151	532	1,141	1,142	1,223
-1,645	-213	869	0.0409	2.289	544	1,179	1,209	1,252
276	-446	957	0.0455	2.406	623	1,178	1,247	1,345
1,528	-937	995	0.0405	2.244	656	994	1,108	1,345
-1,100	-1,673	1,042	0.0472	2.471	571	1,150	1,152	1,438
-1,080	884	1,082	0.0472	2.375	665	1,090	1,167	1,252
302	-1,991	1,081	0.0408	2.616	626	1,175	1,282	1,333
1,726	38	1,484	0.0482	1.800	536	1,054	1,108	1,142
-752	-671	1,487	0.0425	1.773	1155	1,150	1,172	1,178
1,210	-1,568	1,694	0.0501	1.840	585	994	1,068	1,175
145	1,370	1,791	0.0466	2.286	582	1,056	1,113	1,168
-540	-1,835	2,035	0.0486	2.152	716	1,037	1,152	1,256
-1,609	64	2,046	0.0478	2.277	649	1,158	1,209	1,212
1,144	841	2,084	0.0457	2.457	657	1,159	1,168	1,223
-845	1,001	2,141	0.0469	2.407	691	1,090	1,113	1,212
220	-254	2,188	0.0403	2.582	645	1,247	1,269	1,424
1,593	-614	2,302	0.0427	2.139	532	1,054	1,194	1,348
-1,482	-1,054	2,318	0.0463	2.186	510	1,158	1,172	1,256
432	-1,790	2,392	0.0506	1.987	442	1,037	1,068	1,333

Table B-10. XCT data for particles in compact LEU09-M19E.

Centroid (μm)			Volume (mm^3)		Surface distance (μm)	Nearest neighbor (μm)		
x	*y*	*z*	Kernel	Region		1st	2nd	3rd
1,477	-2	790	0.0432	2.227	476	951	1,354	1,423
562	1,087	817	0.0443	2.554	498	1,253	1,361	1,423
-1,341	535	827	0.0456	1.793	510	872	1,031	1,305
86	-379	846	0.0431	2.229	532	935	1,332	1,442
-1,296	-1,333	908	0.0428	2.169	589	1,026	1,060	1,459
377	-1,952	952	0.0439	2.131	634	1,087	1,154	1,172
1,357	-1,321	1,071	0.0445	2.416	628	1,172	1,213	1,330
-767	1,131	1,105	0.0477	2.078	658	872	1,146	1,212
-1,657	-377	1,188	0.0455	1.851	645	969	1,031	1,060
-619	-1,937	1,387	0.0468	1.808	577	932	1,026	1,087
-432	-355	1,623	0.0458	1.650	1053	881	935	1,300
1,575	64	1,733	0.0458	1.907	676	910	951	1,134
79	1,369	1,938	0.0430	2.389	612	1,212	1,253	1,269
616	-1,792	2,070	0.0424	2.288	600	1,154	1,162	1,330
1,215	822	2,086	0.0476	2.094	589	910	1,269	1,425
-1,194	764	2,103	0.0437	2.360	566	1,146	1,305	1,351
-1,654	-505	2,148	0.0455	2.080	521	969	1,338	1,351
257	-230	2,159	0.0454	1.972	510	881	1,332	1,342
1,393	-942	2,223	0.0449	1.973	453	1,134	1,162	1,213
-719	-1,551	2,230	0.0424	2.146	442	932	1,365	1,371

Table B-11. XCT data for particles in compact LEU09-M24E.

Centroid (μm)			Volume (mm^3)		Surface distance (μm)	Nearest neighbor (μm)		
x	***y***	***z***	**Kernel**	**Region**		**1st**	**2nd**	**3rd**
-916	745	785	0.0415	2.221	430	1,138	1,175	1,178
952	542	862	0.0428	1.991	510	1,018	1,020	1,033
163	1,180	949	0.0384	2.181	600	1,018	1,175	1,200
-1,477	-803	969	0.0427	2.247	623	973	1,054	1,363
1,529	-795	1,015	0.0464	2.226	668	1,060	1,140	1,201
61	-617	1,048	0.0443	3.096	702	1,458	1,474	1,479
-756	-1,955	1,073	0.0421	2.356	555	1,101	1,234	1,339
897	-1,807	1,155	0.0449	2.448	612	1,107	1,201	1,281
-1,587	37	1,446	0.0467	1.971	676	902	973	1,178
1,630	139	1,508	0.0449	1.890	612	959	1,020	1,060
956	938	1817	0.0478	2.148	704	991	1,033	1,091
46	-2,039	1,823	0.0487	1.746	645	994	1,065	1,101
-918	964	1,902	0.0487	2.708	697	1040	1,138	1,231
-1,371	-1,280	1,903	0.0448	1.902	666	892	1,054	1,085
1,448	-1,140	2,099	0.0475	2.149	674	974	1,140	1,174
62	1,212	2,147	0.0434	2.496	713	991	1,040	1,203
-1,328	-255	2,258	0.0423	2.901	611	902	1,085	1,335
1,115	-31	2,299	0.0413	2.707	566	959	1,094	1,174
-808	-1,765	2,398	0.0408	1.969	464	892	1,065	1,339
746	-1,717	2,451	0.0457	1.976	419	974	994	1,308

Table B-12. XCT data for particles in compact LEU09-M26E.

Centroid (μm)			Volume (mm^3)		Surface distance (μm)	Nearest neighbor (μm)		
x	*y*	*z*	Kernel	Region		1st	2nd	3rd
-1,218	679	793	0.0452	2.146	464	1,094	1,144	1,359
230	1,103	818	0.0410	2.312	487	1,124	1,196	1,380
60	-283	930	0.0464	2.398	600	896	1,360	1,401
-1,412	-1,179	987	0.0428	2.457	653	1,158	1,279	1,308
-368	-1,975	1,029	0.0430	2.263	620	1,013	1,134	1,314
1,587	7	1032	0.0445	2.385	665	1,073	1,230	1,272
1,443	-1,257	1,047	0.0497	2.334	581	1,111	1,206	1,272
569	-1,847	1,394	0.0411	2.098	680	1,013	1,013	1,111
-1,611	-125	1,422	0.0475	2.036	668	1,046	1,094	1,158
1,185	882	1,505	0.0485	2.126	596	1,073	1,161	1,175
-573	1,166	1,602	0.0445	2.012	688	1,074	1,115	1,124
372	-429	1,757	0.0469	1.763	1053	875	896	1,387
-845	-1,733	2,028	0.0468	2.199	663	1,021	1,134	1,251
-1,362	592	2,142	0.0512	2.288	641	1,046	1,115	1,282
323	1,258	2,187	0.0424	2.439	623	1,074	1,161	1,380
-276	-85	2,234	0.0439	2.098	577	875	1,282	1,360
-1,519	-998	2,249	0.0466	2.065	555	1,021	1,206	1,279
1,458	-1,160	2,248	0.0496	2.104	555	1,206	1,231	1,323
1,566	66	2,261	0.0451	2.275	544	1,175	1,230	1,231
347	-1,864	2,382	0.0436	1.981	430	1,013	1,251	1,323

Table B-13. XCT data for particles in compact LEU09-M29E.

Centroid (μm)			Volume (mm^3)		Surface distance (μm)	Nearest neighbor (μm)		
x	*y*	*z*	Kernel	Region		1st	2nd	3rd
-404	1,157	790	0.0435	2.367	487	1,053	1,066	1,346
1,282	525	805	0.0449	2.398	498	1,014	1,067	1,338
1,353	-1,112	896	0.0416	2.524	589	955	1,054	1,338
-1,494	-513	929	0.0420	2.086	623	900	982	1,021
-1,489	385	993	0.0450	2.169	658	900	1,252	1,264
-96	-1,921	1,003	0.0413	2.514	702	1,068	1,084	1,164
-1,162	-1,462	1,101	0.0469	2.302	673	1,021	1,145	1,164
590	1,168	1,174	0.0415	2.167	707	1,014	1,066	1,086
1,650	-255	1,433	0.0454	1.938	668	1,054	1,067	1,078
859	-1,724	1,438	0.0473	1.853	657	955	997	1,068
-733	1,080	1,787	0.0428	2.000	729	955	989	1,053
-1,698	-465	1,888	0.0495	1.678	605	918	982	1,065
-567	-1,894	1,979	0.0486	1.929	631	1,063	1,084	1,111
27	-348	2,057	0.0458	3.462	736	1,521	1,548	1,568
1,295	574	2,142	0.0439	2.669	657	1,147	1,312	1,336
138	1,193	2,162	0.0468	2.336	634	955	1,086	1,312
1,414	-950	2,223	0.0437	2.409	578	1,078	1,234	1,326
-1,376	485	2,248	0.0438	2.118	555	989	1,065	1,264
434	-1,836	2,333	0.0445	1.918	464	997	1,063	1,326
-1,330	-1,172	2,342	0.0455	1.876	453	918	1,111	1,286

Table B-14. XCT data for particles in compact LEU09-M36E.

Centroid (μm)			Volume (mm^3)		Surface distance (μm)	Nearest neighbor (μm)		
x	***y***	***z***	**Kernel**	**Region**		**1st**	**2nd**	**3rd**
1,431	201	784	0.0440	1.948	419	942	1,101	1,173
-909	884	813	0.0416	2.138	453	951	1,086	1,206
121	1,226	842	0.0393	2.015	476	977	1,086	1,176
-1,649	-601	882	0.0405	2.375	521	1,127	1,170	1,314
675	-1,642	873	0.0405	2.088	510	914	962	1,023
1,372	-894	886	0.0439	2.091	521	1,023	1,024	1,101
-826	-1,830	943	0.0430	2.261	578	1,068	1,072	1,313
874	780	1,276	0.0474	2.015	861	942	977	1,052
-1,414	358	1,424	0.0428	1.816	711	951	995	1,089
71	-2,136	1,435	0.0453	1.566	544	962	1,001	1,039
1,711	-429	1,733	0.0448	1.761	600	1,007	1,024	1,040
-1,248	-1,269	1,754	0.0480	1.946	768	1,031	1,059	1,072
951	-1,765	1,736	0.0433	1.839	616	884	914	1,001
262	1,260	2,009	0.0477	2.392	646	1,069	1,176	1,212
-919	988	2,015	0.0464	2.418	660	995	1,206	1,212
-138	-483	2,094	0.0448	3.335	612	1,402	1,474	1,516
1,345	415	2,143	0.0436	2.294	566	1,007	1,052	1,379
-1,607	-402	2,179	0.0451	2.114	532	1,031	1,089	1,314
-569	-1,930	2,227	0.0449	2.033	476	1,039	1,059	1,313
1,345	-1,217	2,305	0.0426	1.782	396	884	1,040	1,456

Table B-15. XCT data for particles in compact LEU09-M42E.

Centroid (μm)			Volume (mm^3)		Surface distance (μm)	Nearest neighbor (μm)		
x	*y*	*z*	Kernel	Region		1st	2nd	3rd
129	1,128	775	0.0374	1.934	430	965	1,074	1,334
-1,573	-581	899	0.0413	2.135	555	1,040	1,076	1,305
-1,101	635	931	0.0485	2.389	589	1,073	1,234	1,305
1,108	705	903	0.0388	2.210	566	1,074	1,152	1,240
35	-401	978	0.0446	2.495	634	1,121	1,478	1,537
1,608	-426	991	0.0400	2.575	657	1,240	1253	1,281
-253	-1,914	1,055	0.0418	2.247	713	1,089	1,094	1,094
810	-1,655	1,093	0.0469	2.524	747	1,032	1,094	1,338
-1,264	-1,548	1,257	0.0432	2.044	563	1,076	1,094	1,142
-419	1,165	1,569	0.0408	1.840	734	904	965	1,073
-1,582	-229	1,878	0.0474	1.997	719	938	1,028	1,040
1,405	-1,334	1,872	0.0422	1.935	591	963	1,032	1,209
1,413	684	2,013	0.0423	2.339	556	1,152	1,207	1,253
108	-306	2,092	0.0421	2.875	702	1,121	1,553	1,573
302	1,255	2,107	0.0441	2.493	671	904	1,253	1,349
-405	-1,809	2,128	0.0459	2.047	668	908	1,089	1,209
-1,351	641	2,139	0.0421	2.363	635	938	1,211	1,234
1,644	-478	2,243	0.0457	1.981	555	963	1,207	1,253
-1,395	-1,141	2,316	0.0445	1.983	487	1,028	1,142	1,209
467	-1,922	2,358	0.0461	1.873	442	908	1,209	1,338

Table B-16. XCT data for particles in compact LEU11-M01B.

Centroid (μm)			Volume (mm^3)		Surface distance (μm)	Nearest neighbor (μm)		
x	***y***	***z***	**Kernel**	**Region**		**1st**	**2nd**	**3rd**
-1,156	-13	827	0.0683	1.902	476	946	1,046	1,330
-295	-1,939	852	0.0727	2.050	498	944	1,231	1,373
1,066	-1,678	913	0.0757	1.880	566	972	1,057	1,387
131	1,306	930	0.0719	2.025	578	1,001	1,142	1,296
1,600	58	937	0.0669	1.970	589	995	1,040	1,231
44	-552	1,025	0.0742	2.487	668	1,176	1,330	1,438
-951	978	1,091	0.0718	2.132	647	1,046	1,142	1,227
925	786	1,247	0.0754	2.119	815	1,001	1,021	1,040
-1,738	-569	1,325	0.0827	2.164	549	946	1,013	1,252
1,598	-860	1,321	0.0778	1.826	624	995	1,055	1,057
-925	-1,693	1,511	0.0758	2.059	675	944	1,003	1,068
537	-1,706	1,728	0.0785	1.840	852	955	972	1,016
-167	107	1,976	0.0772	2.018	725	437	1,111	1,176
-1,461	-1,116	2,131	0.0769	2.206	578	1,003	1,013	1,469
-1,451	353	2,123	0.0702	2.222	589	1,000	1,252	1,306
-320	1,195	2,139	0.0774	1.949	566	787	1,111	1,242
1,540	3	2,165	0.0754	2.190	544	1,126	1,209	1,231
1,335	-1,325	2,230	0.0760	2.049	476	1,016	1,055	1,346
-208	-2,048	2,218	0.0596	1.983	487	955	1,068	1,373
949	959	2,252	0.0771	1.899	453	1,021	1,126	1,296

Table B-17. XCT data for particles in compact LEU11-M05B.

Centroid (μm)			Volume (mm^3)		Surface distance (μm)	Nearest neighbor (μm)		
x	*y*	*z*	Kernel	Region		1st	2nd	3rd
-1,046	-1,573	828	0.0753	2.065	487	1,083	1,114	1,221
632	-1,782	828	0.0748	1.998	487	1,042	1,094	1,278
-1,310	133	872	0.0729	2.222	532	1,009	1,058	1,305
71	-326	893	0.0782	2.422	555	1,205	1,410	1,456
1,411	-764	879	0.0662	2.130	544	1,043	1,093	1,283
1,152	838	894	0.0694	2.246	555	1,115	1,123	1,315
-352	1,196	940	0.0650	2.408	600	1,101	1,230	1,243
-1,589	-731	1,313	0.0727	1.952	665	998	1,009	1,114
-219	-1,972	1,401	0.0707	1.875	671	977	1,042	1,083
1,680	80	1,519	0.0771	1.761	571	1,057	1,072	1,093
1,358	-1,513	1,602	0.0718	1.567	512	946	1,043	1,072
469	1,281	1,669	0.0760	1.801	607	1,020	1,066	1,101
-1,196	741	1,731	0.0661	2.056	689	1,012	1,040	1,058
-1,130	-1,541	2,046	0.0707	2.516	623	1,185	1,197	1,221
147	-270	2,095	0.0760	2.633	578	1,205	1,470	1,552
450	-1,802	2,093	0.0709	2.258	578	977	1,072	1,278
-1,600	-137	2,115	0.0791	2.163	555	998	1,040	1,305
1,610	-784	2,149	0.0808	1.882	521	946	1,072	1,286
-418	1,218	2,168	0.0802	1.884	510	1,012	1,020	1,230
1,213	736	2,204	0.0760	1.932	464	1,057	1,066	1,315

Table B-18. XCT data for particles in compact LEU11-M14B.

Centroid (μm)			Volume (mm^3)		Surface distance (μm)	Nearest neighbor (μm)		
x	*y*	*z*	Kernel	Region		1st	2nd	3rd
-1,432	-1,122	826	0.0649	2.068	521	1,116	1,116	1,300
847	-1,513	824	0.0665	1.809	521	963	981	1,206
-1,101	667	842	0.0683	2.239	532	1,067	1,093	1,288
338	1,258	859	0.0632	2.236	555	1,062	1,176	1,261
1,543	67	886	0.0764	2.150	578	1,067	1,121	1,257
25	-303	932	0.0694	2.519	623	1,149	1,466	1,489
-320	-1,780	970	0.0807	2.329	668	1,180	1,197	1,206
1,634	-989	1,008	0.0689	1.767	541	963	1,067	1,112
-1,664	-128	1,276	0.0761	1.997	629	1,001	1,067	1,116
1,157	949	1,460	0.0703	1.761	593	1,028	1,061	1,062
-567	1,231	1,611	0.0771	1.993	659	1,014	1,093	1,132
698	-1,910	1,709	0.0765	1.845	567	981	995	1,135
-1,143	-1,595	1,795	0.0685	2.013	593	1,059	1,116	1,133
165	-86	2,052	0.0712	2.471	600	1,149	1,404	1,412
1,343	-1,053	2,079	0.0751	2.285	566	1,112	1,135	1,288
-1,297	738	2,113	0.0801	2.079	532	1,014	1,259	1,285
444	1,297	2,115	0.0691	1.976	532	1,028	1,132	1,261
1,533	220	2,134	0.0788	2.093	521	1,061	1,257	1,288
-1,386	-544	2,143	0.0749	2.197	510	1,001	1,133	1,285
-190	-1,883	2,156	0.0717	1.974	498	995	1,059	1,197

APPENDIX C.

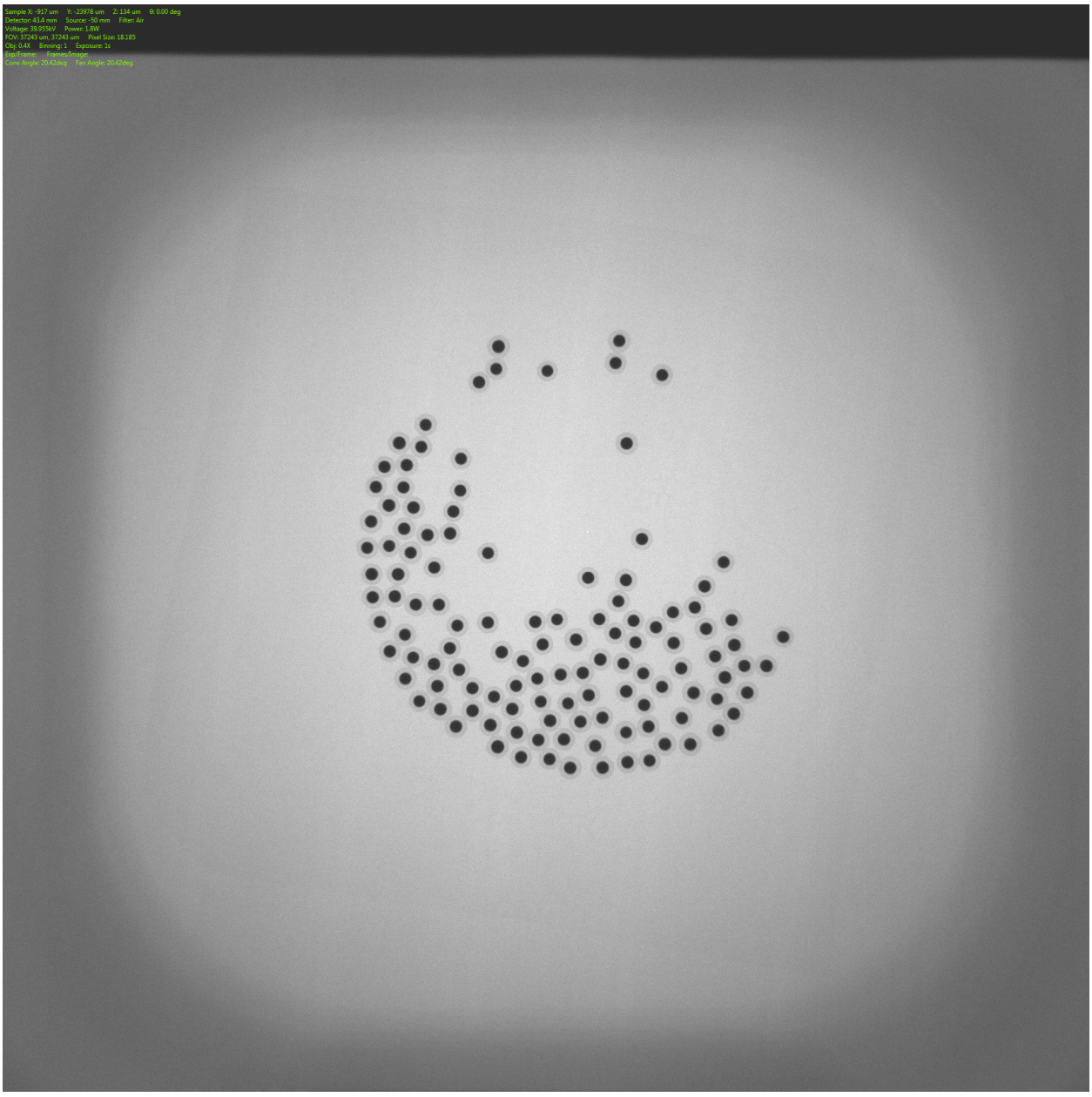

Figure C-1. Radiograph of burn test clutch #1 from LEU09-M##E.

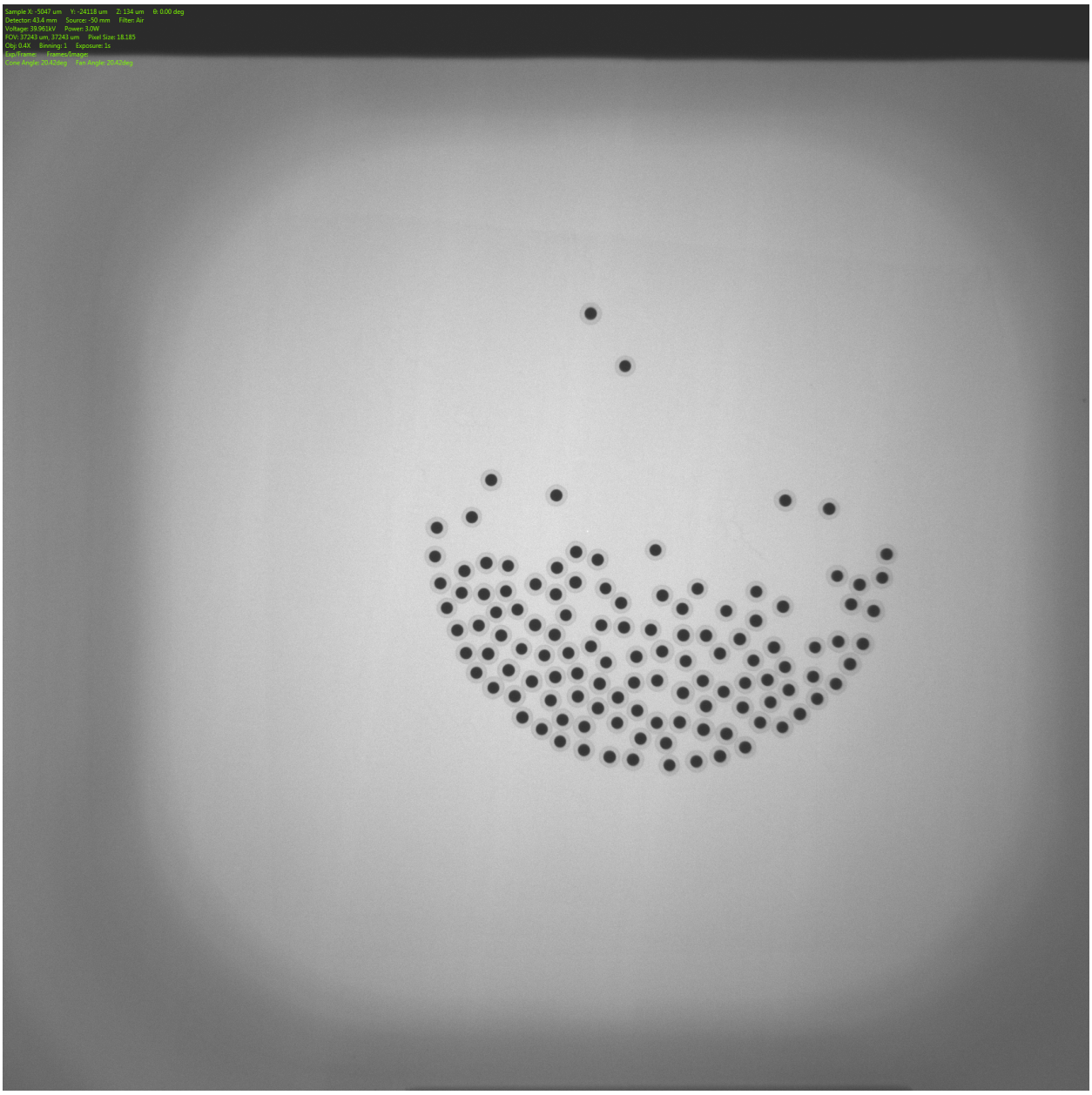

Figure C-2. Radiograph of burn test clutch #2 from LEU09-M##E.

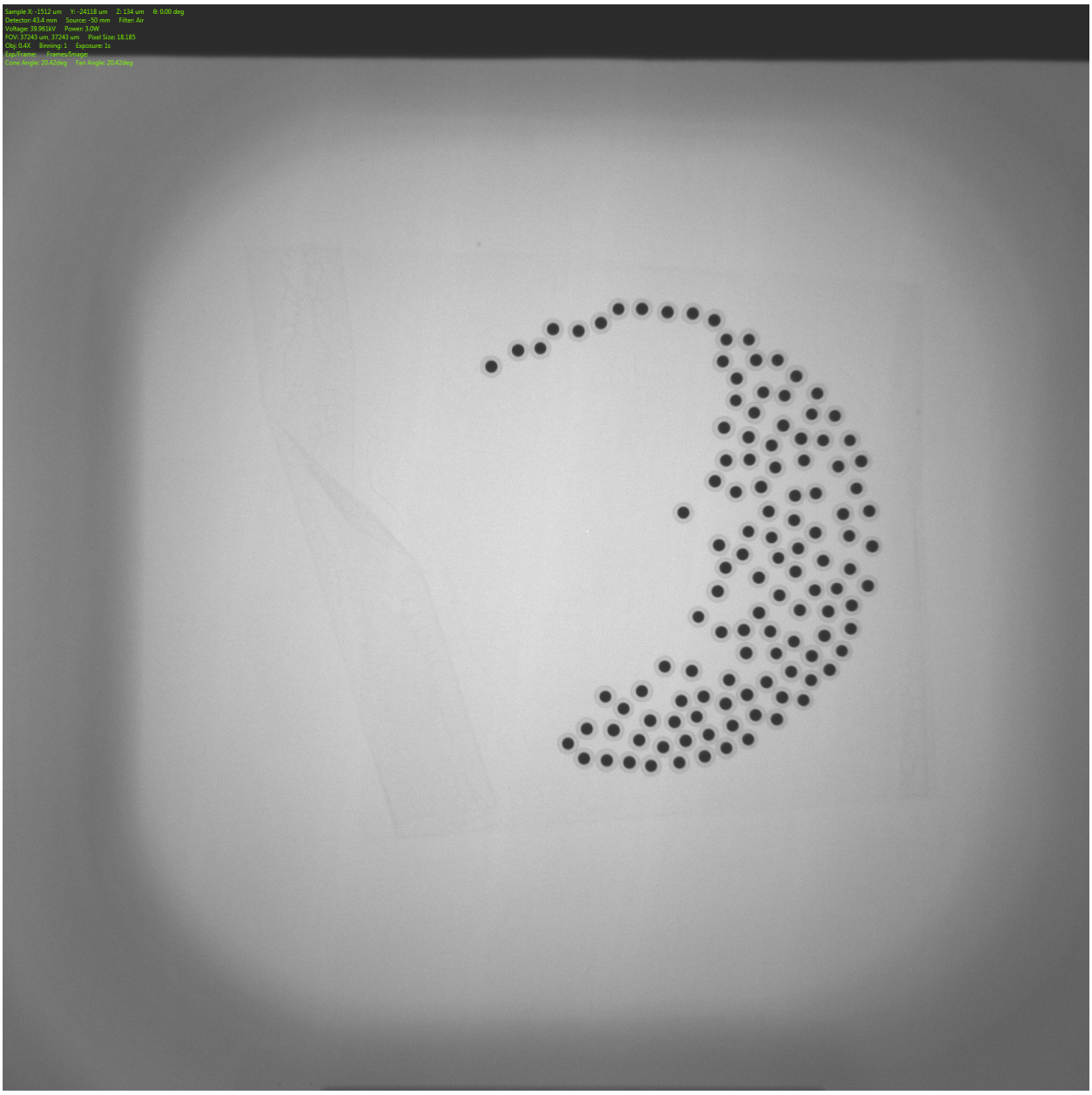

Figure C-3. Radiograph of burn test clutch #3 from LEU09-M##E.

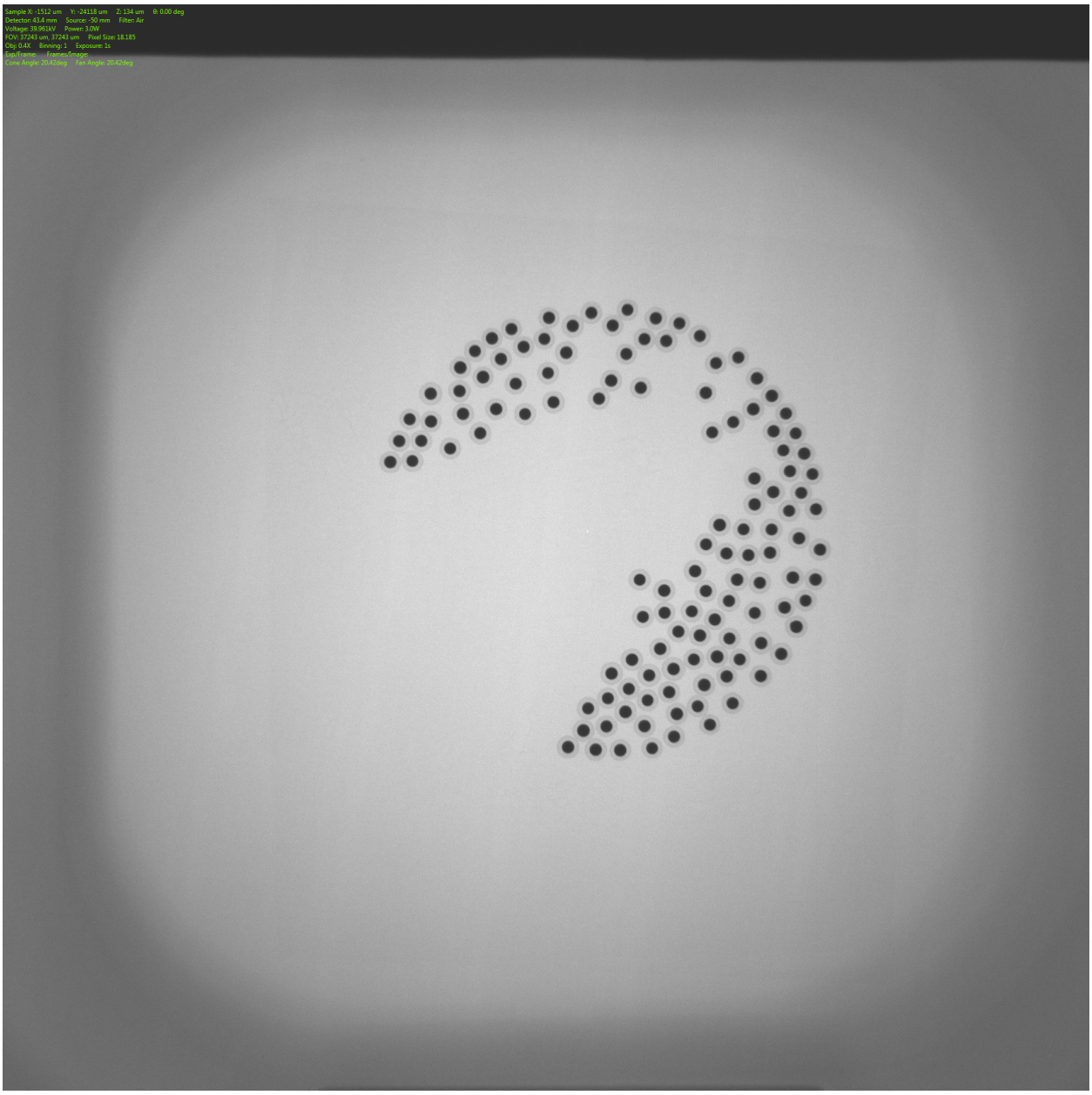

Figure C-4. Radiograph of burn test clutch #1 from LEU09-M##G.

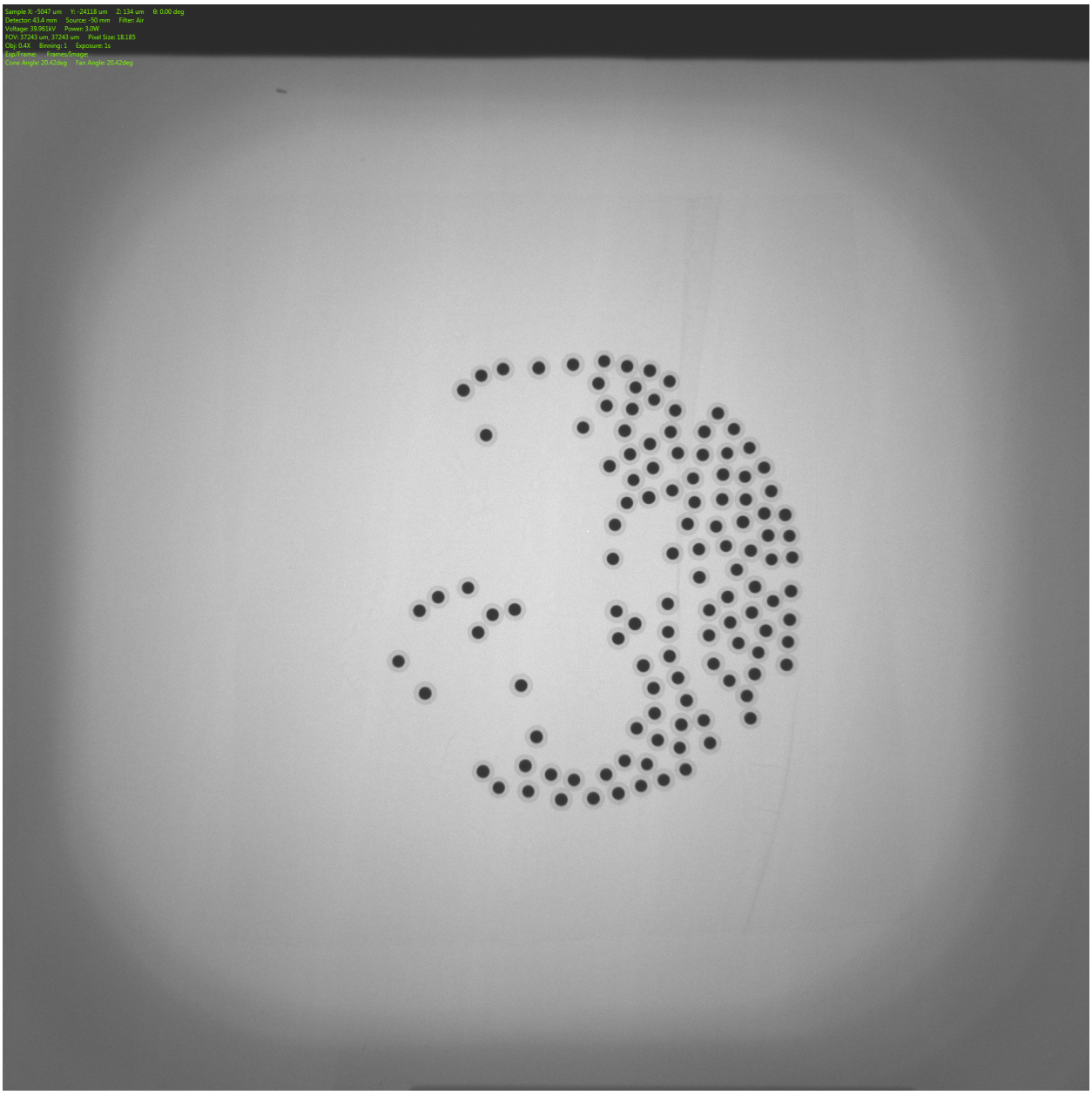

Figure C-5. Radiograph of burn test clutch #2 from LEU09-M##G.

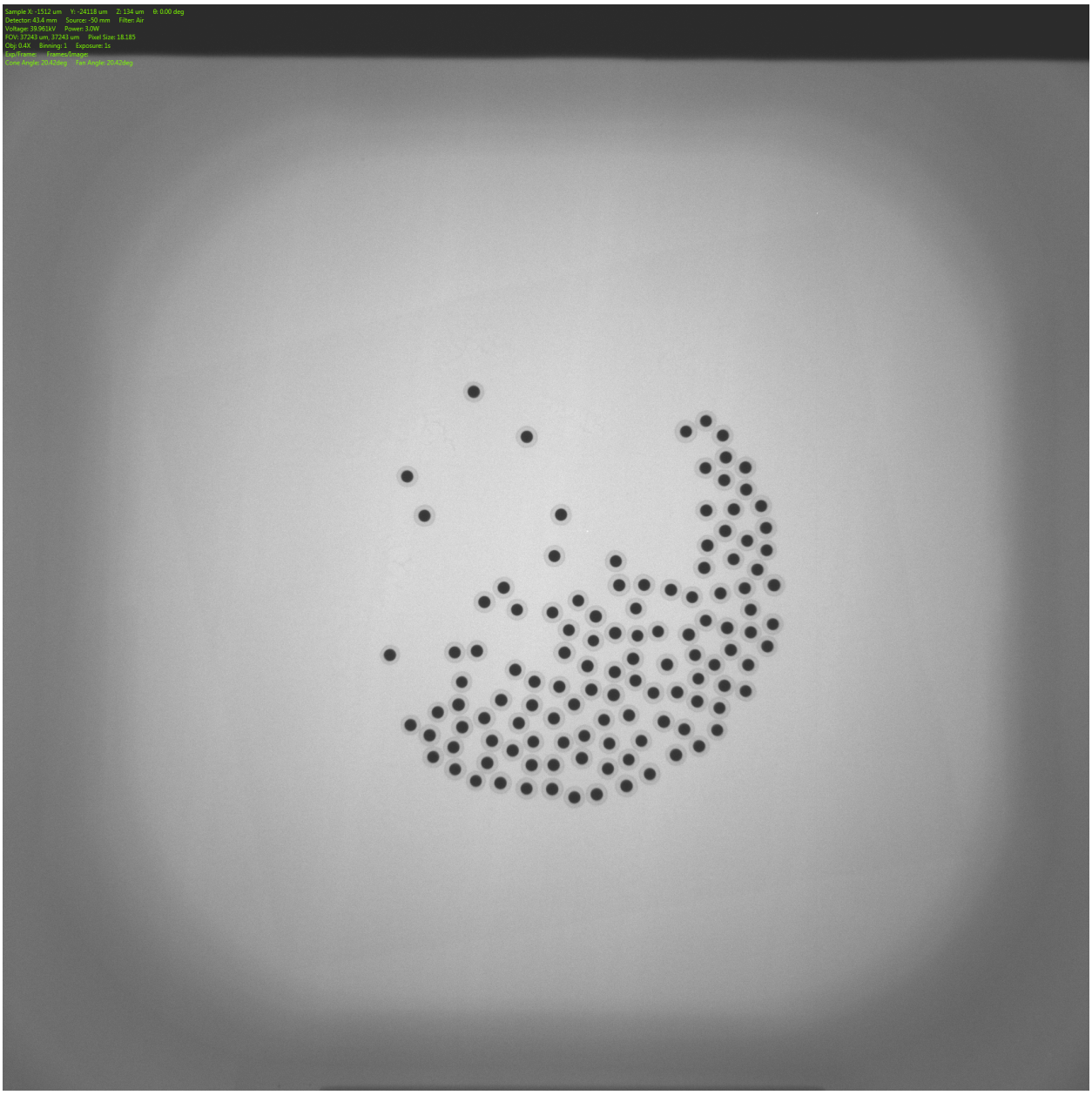

Figure C-6. Radiograph of burn test clutch #3 from LEU09-M##G.

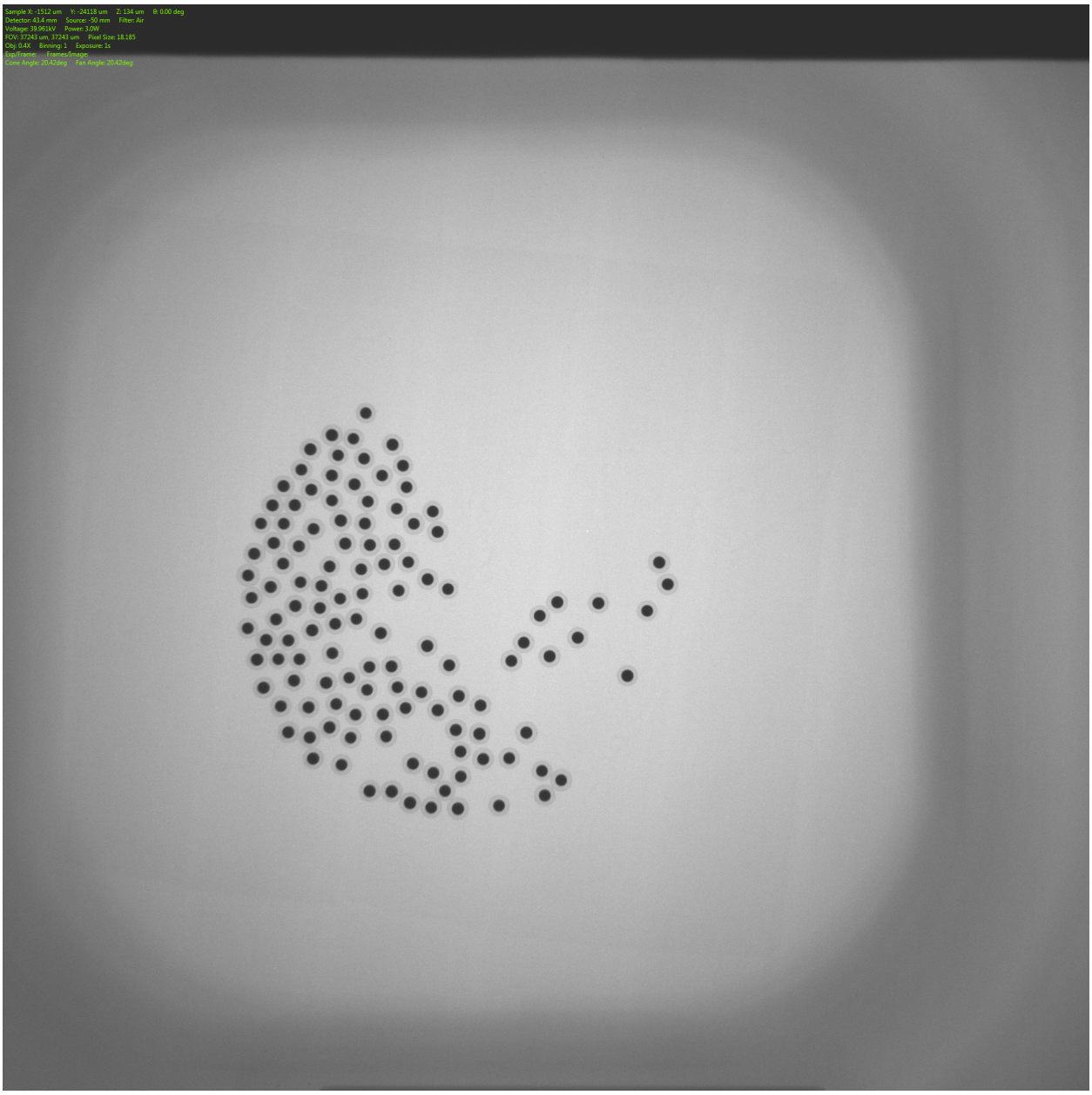

Figure C-7. Radiograph of burn test clutch #4 from LEU09-M##G.

Figure C-8. Radiograph of burn test clutch #5 from LEU09-M##G.

Figure C-9. Radiograph of burn test clutch #6 from LEU09-M##G.

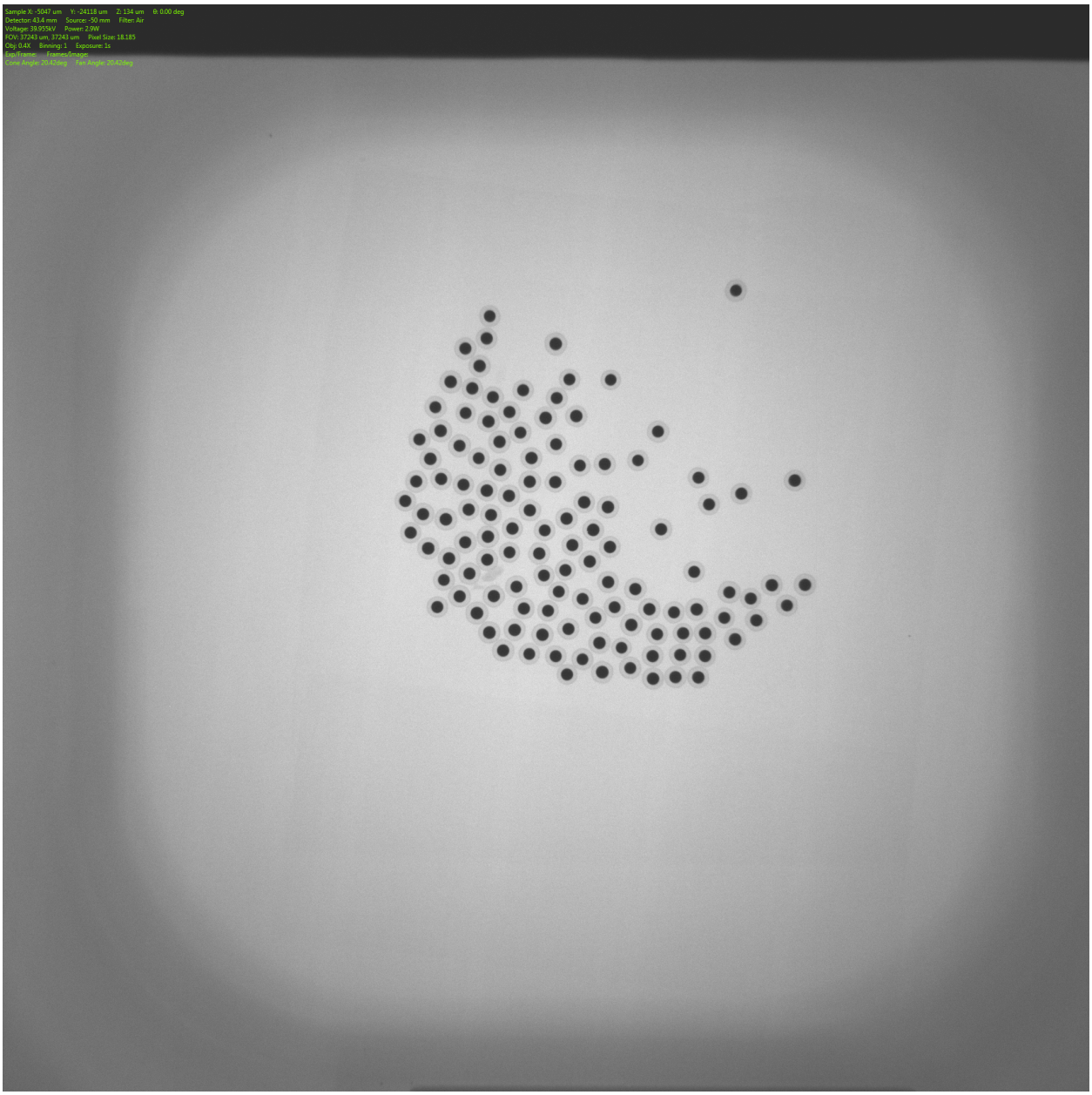

Figure C-10. Radiograph of burn test clutch #7 from LEU09-M##G.

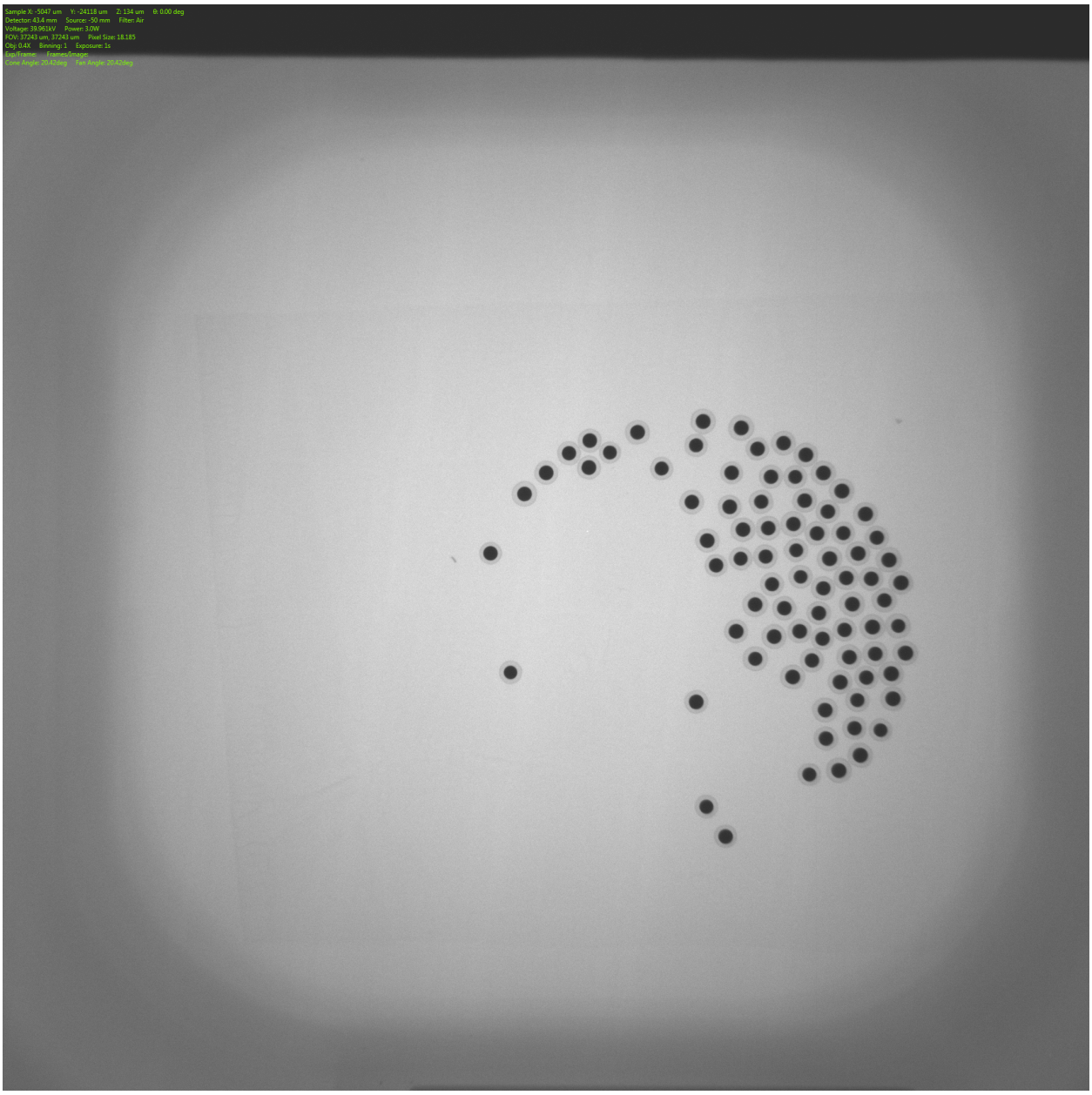

Figure C-11. Radiograph of burn test clutch #1 from LEU11-M##B.

Figure C-12. Radiograph of burn test clutch #2 from LEU11-M##B.

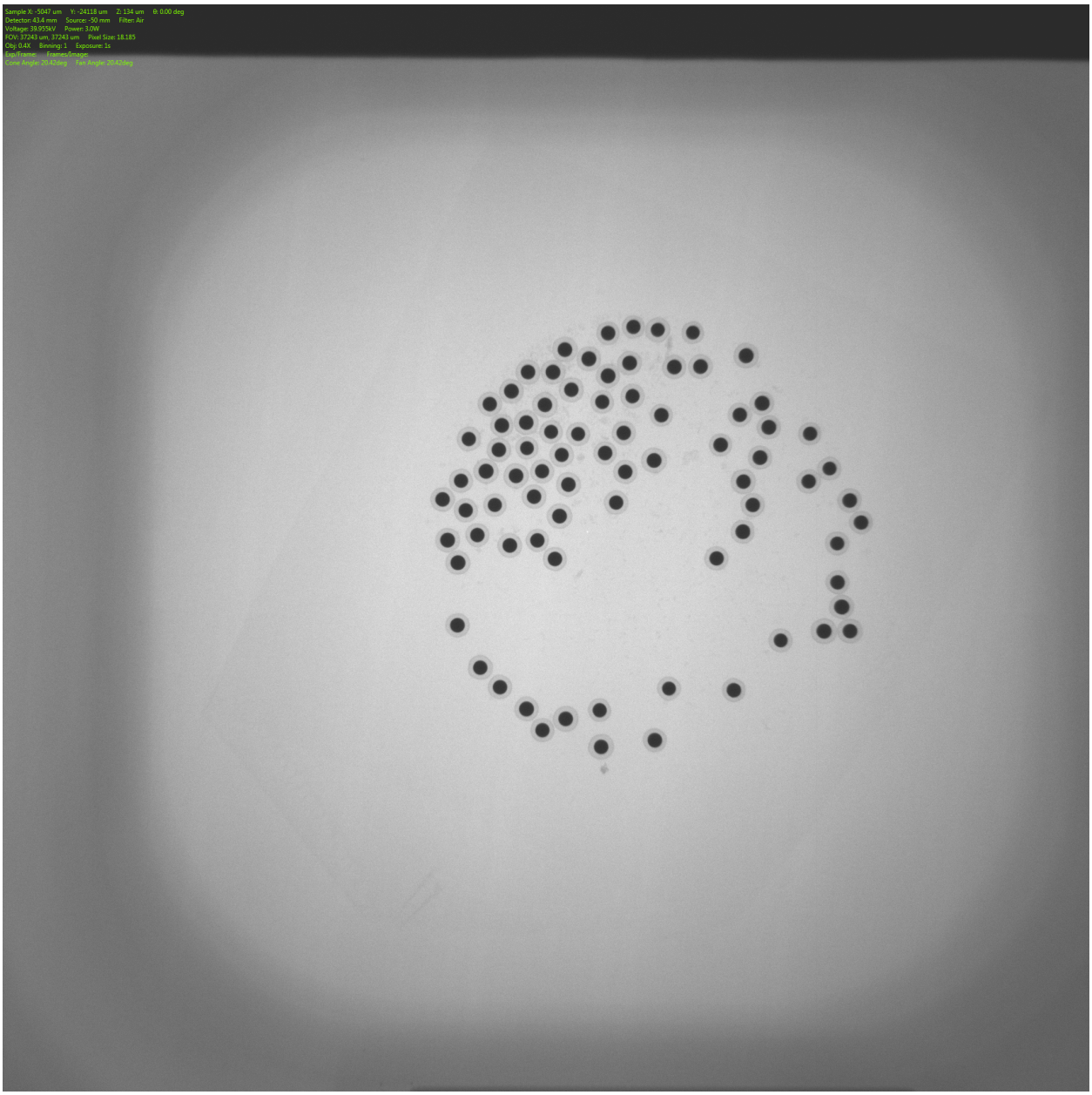

Figure C-13. Radiograph of burn test clutch #3 from LEU11-M##B.